The physical and chemical processes in protoplanetary disks: constraints on the composition of comets

Yuri Aikawa
Department of Astronomy, The University of Tokyo

Satoshi Okuzumi
Department of Earth and Planetary Sciences, Institute of Science Tokyo

Klaus Pontoppidan
Jet Propulsion Laboratory

We review the recent observations of protoplanetary disks together with relevant theoretical studies with an emphasis on the evolution of volatiles. In the last several years *Atacama Large Millimeter/submillimeter Array* (ALMA) provided evidence of grain growth, gas-dust decoupling, and sub-structures such as rings and gaps in the dust continuum. Molecular line observations revealed radial and vertical distributions of molecular abundances and also provided significant constraints on the gas dynamics such as turbulence. While sub-millimeter and millimeter observations mainly probe the gas and dust outside the radius of several au, ice and inner warm gas are investigated at shorter wavelengths. Gas and dust dynamics are key to connect these observational findings. One of the emerging trends is in-homogeneous distributions of elemental abundances, most probably due to dust-gas decoupling.

1. INTRODUCTION

Planetary systems, including our Solar system, are formed in protoplanetary disks, which are circumstellar disks around pre-main-sequence stars. Since COMET II, new astronomical instruments, such as ALMA and *Herschel Space Observatory*, made dramatic progress in the observation of protoplanetary disks. In particular, ALMA made it possible to observe the thermal emission of dust grains with a spatial resolution of 5 au in the disks in the solar neighborhood (e.g. the Ophiuchus star-forming region). The discovery of the ring-gap structure stimulated theoretical studies on grain growth and planetesimal formation processes. Various gas molecules such as CO, on the other hand, are observed with a spatial resolution of ~ 15 au. Observations of these molecules provide an important clue to unveil the composition of ice, which, together with dust, is the ingredient of comets. In this chapter, we review the progress of these observational and theoretical studies of protoplanetary disks, which serve as references to investigate the comet formation in the Solar nebula.

Before proceeding to the main sections, we briefly explain the process of star formation in order to set up the stage and to clarify the relationship with the chapter by Bergin et al. Low-mass stars like the Sun are formed by the gravitational collapse of a molecular cloud core. Since the core has non-zero angular momentum as a whole, the central star and its circumstellar disk are formed simultaneously. In the early stages, the star and disk are deeply embedded in dense gas, which we call envelope. Since the envelope is cold, the spectral energy distribution (SED) of the object has a peak in the far infrared. The objects in this evolutionary stage are called Class 0. In spite of its low temperature at the outermost radius of the envelope, the temperature of the forming disk would be high due to the high mass accretion rate inside the disk (i.e. release of gravitational energy), and shock heating caused by accretion from the envelope to the disk (e.g. *Offner and McKee* 2011, see also Fig. 1 and §2.2). While the envelope gas accretes to the central star via disk, the high-velocity jet and outflow are launched from the vicinity of the central star. Eventually, the envelope gas decreases as it falls to the disk and star, or it is swept by the jet and outflow. When the central star (i.e. in near-infrared wavelengths) becomes apparent in the SED, which is still dominated by mid- to far-infrared though, the objects are called Class I. Eventually, when the envelope gas is dissipated, the central star becomes a T Tauri star and the disk becomes a protoplanetary disk, which is also called Class II disk. More detailed explanations and quantitative definitions of Class 0, I, and II are found in *Evans et al.* (2009).

While it is not easy to determine the age of pre-main-sequence stars, the typical age of the Class II objects is a few 10^6 years. Statistical observations (i.e. number counts) indicate that the lifetime for Class 0 and Class I is $\sim 0.1 - 0.2$ Myr and $\sim 0.4 - 0.5$ Myr, respectively (e.g. *White et al.* 2007; *Evans et al.* 2009). In order to set Solar system formation in an astronomical context, these timescales are compared with the range of absolute ages (i.e. formation interval) of Calcium and Aluminium Inclusions (CAIs) and chondrules in meteorites. CAIs have the highest condensation temperature among minerals in chondrites and are thus considered to be formed in the hottest stage and/or region. The formation interval of CAIs is estimated to be 0.16 Myr by the isotope dating, which is com-

parable to the lifetime of Class 0 stage. The age of the chondrules, on the other hand, varies over a few Myr, which coincides with the lifetime of Class II disks (*Connelly et al.* 2012). While Class II disks have been considered to be the birthplace of planetary systems, a ring-gap structure of dust thermal emission is recently found in some Class I disks as well. It suggests that planetary system formation may start early (see §4). In summary, the Solar nebula may correspond to the whole evolutionary stages from Class 0, I, and to II.

Having said that, in this chapter, we focus our attention on Class II disks. Chondrule fragments found in the sample return mission of Comet Wild 2 indicate the formation of comets during or after the chondrule formation (*Bridges et al.* 2012), i.e. in Class II disks. The physical and chemical processes and structures in Class II disks are better understood as depicted in Fig. 1 compared with the younger disks, which need more careful analysis to be distinguished from the accreting envelope gas and outflows (e.g. *van Dishoeck et al.* 2021). In §2, we describe the physical structure and processes in disks such as temperature distributions and gas dynamics, which are of fundamental importance for chemistry and comet formation in disks. Since comets contain significant amounts of volatiles such as water ice, they are considered to be formed in low-temperature regions outside the snowline. In §3 we review the basic chemical structure of the disk and recent observations of molecular gas and ice at various wavelengths, as well as the studies on isotope fractionation in disks. The chemical properties of disk material provide a reference for investigations of the formation and evolution of comets based on their volatile composition and isotope ratios. In §4 we overview two outstanding issues on disk chemistry; the chemical evolution of volatiles from earlier phases (Class 0 and I) to Class II disks, and how and what we can learn about volatiles in solids from line observations of disks and central stars.

2. Physical processes in protoplanetary disks

In this section, we describe the basic physical structure and relevant observational results. The radial temperature distribution in disks determines snowlines, outside of which specific volatile species will be in ice to be incorporated into comets. Vertical temperature structure is also important to interpret the disk observations. The major heating source is stellar irradiation and gravitational energy released by the mass accretion towards the central star. Both the stellar luminosity and mass accretion rate are expected to vary with time, which results in temporal variation of the snowlines. Mass accretion, in turn, is determined by the angular momentum transfer within the disk, which could be caused by turbulence and/or disk winds (Fig.1). We note that angular momentum transfer and turbulence will also determine how the ingredients of comets, ices and grains, are mixed and distributed within the disk. We thus start this section with gas dynamics. Later in this section, we also provide the current overview of dust observations. Observations indicate that dust grains have grown at least to 100 μm, and possibly to larger sizes. As grains grow, they decouple from the gas. Large grains, called pebbles, lose or gain angular momentum via gas drag to radially migrate, and are concentrated at a local gas pressure maximum. Such dust rings (and gaps) are found in many disks in the last several years.

2.1. Gas dynamics

Pre-main-sequence stars accrete material from their surrounding disks. For solar-mass pre-main-sequence stars, the mass accretion rates estimated from observations are on average $\sim 10^{-8}$ $\mathrm{M_\odot\ yr^{-1}}$ at a stellar age t of ~ 1 Myr and crudely scale inversely with t (*Hartmann et al.* 2016). Some pre-main-sequence stars show months-long and decades-long luminosity eruptions, called EX Ori and FU Ori outbursts, with estimated accretion rates of $\sim 10^{-7} M_\odot\ \mathrm{yr}^{-1}$ and $\sim 10^{-5}$–$10^{-4} M_\odot\ \mathrm{yr}^{-1}$, respectively (*Hartmann et al.* 2016; *Fischer et al.* 2023).

The observed stellar accretion indicates that the inner region of disks loses angular momentum. What mechanisms are responsible for the angular momentum transport is a long-standing question in the study of protoplanetary disk evolution. Classically, the accretion of protoplanetary disks as well as other astrophysical accretion disks was attributed to outward angular momentum transport within the disks by turbulence (*Lynden-Bell and Pringle* 1974). However, as we detail below, neither theory nor observations support the picture that protoplanetary disks are strongly turbulent everywhere.

On the theoretical side, it was previously thought that the magnetorotational instability (MRI; *Balbus and Hawley* 1991) is a major cause of protoplanetary disk turbulence. The MRI is most likely to operate in the innermost disk regions where the gas is hot (≥ 1000 K) and thermally well-ionized (*Gammie* 1996; *Desch and Turner* 2015). However, farther out in the disks, the gas is only poorly ionized and the magnetohydrodynamics (MHD) is strongly subject to magnetic diffusion (*Sano et al.* 2000; *Ilgner and Nelson* 2006; *Wardle* 2007; *Bai* 2011). Recent theoretical studies (*Bai* 2011; *Bai and Stone* 2013; *Simon et al.* 2013a,b; *Lesur et al.* 2014; *Gressel et al.* 2015; *Bai* 2017) have shown that while Ohmic diffusion suppresses the MRI near the disk midplane, ambipolar diffusion (which is a type of magnetic diffusion occurring in low-density regions) also suppresses the MRI well above the midplane. In the inner few au of the disks, the combined effect of the Ohmic and ambipolar diffusion can quench the MRI at all heights (*Bai* 2013).

From the observational side, direct constraints on disk turbulence strength have been obtained from measurements of nonthermal Doppler broadening of molecular emission lines (*Hughes et al.* 2011; *Guilloteau et al.* 2012). Recently, there have been several attempts to detect disks' nonthermal gas motions using ALMA, but most of them have resulted in non-detection with upper limits on the nonthermal velocity dispersion of several to ten % of the local sound speed

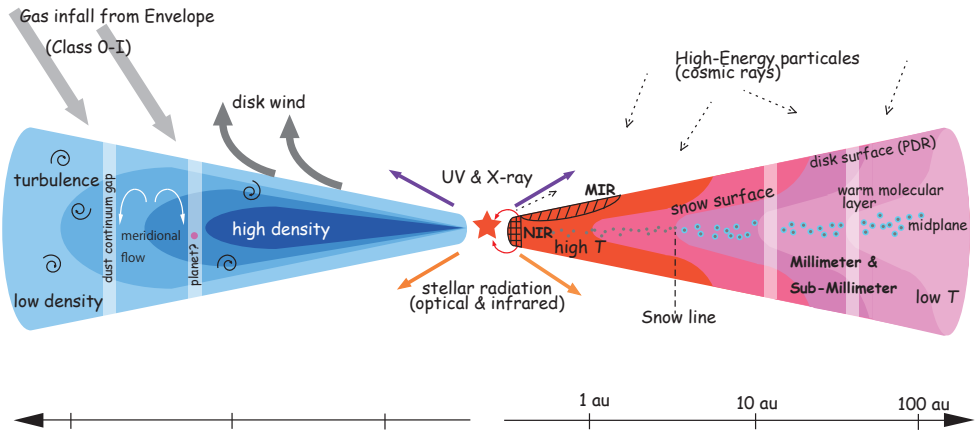

Fig. 1.— Schematic view of the disk structure. The physical structures and processes are shown on the left: density distribution (blue contour), weak turbulence, disk wind, gaps seen in dust continuum emission, and meridional flow. In early disk-forming stages (Class 0 and I), we also have gas accretion from the envelope. The temperature distribution (red contour) is depicted on the right, together with the basic chemical structures: disk surface irradiated by UV radiation, warm molecular layer, and midplane. Snow surface is defined as the boundary outside which the dust temperature is lower than the sublimation temperature of a volatile molecule. Snow line is the intersection between the snow surface and the disk midplane. Infrared observations trace hot regions at the inner radius and disk surface, while millimeter and sub-millimeter observations probe the outer ($\geq$ 5 au) regions.

(*Flaherty et al.* 2015, 2017, 2018; *Teague et al.* 2016, 2018). To date, the disks around DM Tau (*Flaherty et al.* 2020) and IM Lup (*Paneque-Carreño et al.* 2024; *Flaherty et al.* 2024) are the only cases for which turbulent motion has been detected with ALMA , albeit at a few gas scale heights above the midplane. There are indirect constraints on turbulence strength at the midplane from the morphology or azimuthal emission variation of dust rings and gaps seen in ALMA millimeter continuum images (*Pinte et al.* 2016; *Dullemond et al.* 2018; *Rosotti et al.* 2020; *Doi and Kataoka* 2021; see Sect. 2.5 for more detail about disk substructures found by millimeter observations). Some rings show an indication of strong vertical settling or radial dust concentration, suggesting that the turbulence at the midplane of the disks is too weak to diffuse the dust particles. However, constraining the level of turbulence quantitatively from these observations requires additional constraints on the dust particle size because large dust particles may settle and concentrate even in the presence of strong turbulence.

While the turbulence is found to be weak, we still need angular momentum transport to account for the mass accretion from the disk to the central star. Various mechanisms are proposed and investigated. The Keplerian shear of the gas disk amplifies large-scale horizontal magnetic fields even when Ohmic diffusion suppresses the MRI (*Turner and Sano* 2008). The Keplerian shear, when coupled to the Hall drift of magnetic fields, also leads to exponential amplification of horizontal magnetic fields, the phenomenon called the Hall-shear instability (*Kunz* 2008), which becomes prominent in inner disk regions (*Bai* 2014, 2017; *Lesur et al.* 2014). Importantly, MHD simulations show that these mechanisms produce *coherent* horizontal magnetic fields with no appreciable level of turbulence. In other words, they induce angular momentum transport leading to large-scale disk accretion but would not cause small-scale mixing of disk material.

Large-scale magnetic fields threading the disks induce another important dynamical phenomenon: disk winds. Protoplanetary disks are thought to inherit magnetic flux from their parent molecular clouds. Depending on the strength and inclination of the threading magnetic fields, the centrifugal force along the field lines or the magnetic field pressure in the vertical direction can accelerate the material on the disk surface to the escape velocity (*Blandford and Payne* 1982; *Shibata and Uchida* 1986). The magnetically driven winds also induce gas accretion *within the disks* because the magnetically accelerated wind material takes away the disks' angular momentum. Recent MHD simulations have shown that the wind-driven accretion alone can account for the observed accretion rates for protoplanetary disks if the magnetic fields vertically threading the disks are sufficiently strong (*Bai and Stone* 2013; *Bai* 2013; *Simon et al.* 2013a; *Lesur et al.* 2014; *Gressel et al.* 2015). However, lacking direct measurements of the strength of disks' large-scale magnetic fields (although there are some constraints on Solar nebula magnetic field strengths from paleomagnetic measurements of meteorites; see *Fu et al.* 2014; *Wang et al.* 2017), it is unclear whether realistic protoplanetary disks can retain the required amount of the vertical magnetic flux. There are several recent theoretical studies

in this direction (*Guilet and Ogilvie* 2014; *Okuzumi et al.* 2014; *Takeuchi and Okuzumi* 2014; *Bai and Stone* 2017; *Zhu and Stone* 2018; *Leung and Ogilvie* 2019).

There are purely hydrodynamical (i.e, non-MHD) instabilities that can produce weak turbulence, including the vertical shear instability (*Urpin and Brandenburg* 1998; *Nelson et al.* 2013), convective overstability (*Klahr and Hubbard* 2014; *Lyra* 2014), and zombie vortex instability (*Marcus et al.* 2015). These hydrodynamical instabilities operate in different ranges of the gas cooling timescale and hence in different disk regions, with the vertical shear instability being most relevant to cold outer disk regions where comets form (*Malygin et al.* 2017; *Lyra and Umurhan* 2019). According to hydrodynamical simulations, turbulence driven by these instabilities does transfer the disk's angular momentum radially, but its transport efficiency appears to be low compared to strong MRI-driven turbulence and magnetically driven winds (*Lyra and Umurhan* 2019). This does not mean that hydrodynamical instabilities are negligible because they can play a significant role in the transport of disk material. For instance, the vertical shear instability produces vertically elongated turbulent eddies that strongly diffuse gas and dust in the vertical direction (*Flock et al.* 2020). The hydrodynamical instabilities also cause the formation of gas pressure bumps and vortices that can efficiently trap dust particles (*Flock et al.* 2020; *Raettig et al.* 2021).

Massive planets also have interesting effects on disk gas dynamics. Early theoretical studies already predicted that a planet larger than Neptune can carve an annular density deficit called a gap in the background gas disk (*Lin and Papaloizou* 1993). Recent three-dimensional simulations have shown that a massive planet also induces meridional (i.e., radial and vertical) flows of the disk gas both inside and outside the gap (*Morbidelli et al.* 2014; *Fung and Chiang* 2016) (Fig. 1). Signatures of the meridional flow are obtained from a detailed analysis of high-resolution molecular line data (*Teague et al.* 2019). The gaps and meridional flows induced by massive planets have important implications for dust evolution (see Sect. 2.3).

2.2. Temperature distribution and snowlines

As in the present-day Solar system, the temperature in protoplanetary disks generally decreases with orbital radius. Therefore, each chemical species in a disk has a critical radius inside which its solid form is unstable. For volatile species, these critical radii are called the snowlines. Because different volatile species have different sublimation temperatures, each of them has its own snowline. [Considering the temperature gradient in the vertical direction, the boundary is actually a snow surface. The snowline is an intersection between the snowsurface and the disk midplane as depicted in Fig 1. We focus on the snowline here, because the midplane dominates in the mass distribution.]

The snowlines are generally expected to affect the radial distribution of volatiles in solids and also in the gas (*Hayashi* 1981; *Öberg et al.* 2011). If we fully understand where the snowlines are and how they move with time, we will be able to constrain where and when planets and comets of different compositions form in disks.

Themodynamically, the snowline of each volatile species can be defined as the location where its saturation vapor pressure equals its partial pressure in the gas phase. To illustrate how the locations of the snowlines are determined, we plot in Fig. 2 the saturation vapor pressure curves for pure CO, $\mathrm{CO_2}$, $\mathrm{NH_3}$, and $\mathrm{H_2O}$ ices as a function of radial distance r for the classical, optically thin minimum-mass Solar nebula (MMSN) model of *Hayashi* (1981), which has radial temperature and midplane pressure profiles of $T_{\mathrm{MMSN}} = 280(r/1\ \mathrm{au})^{-1/2}$ K and $P_{\mathrm{MMSN}} = 1.4(r/1\ \mathrm{au})^{-13/4}$ Pa, respectively. Here, we adopt analytic expressions for the saturation vapor pressures as a function of temperature provided by *Bauer et al.* (1997) (for $\mathrm{H_2O}$) and by *Yamamoto et al.* (1983) (for the other species), and plot them as a function of r using the assumed temperature profile. Let us assume that the disk contains CO, $\mathrm{CO_2}$, $\mathrm{NH_3}$, and $\mathrm{H_2O}$ at spatially uniform molar abundances of $f = 10^{-4}$, 10^{-4}, 10^{-5}, and 10^{-3}, respectively, so that the relative abundances between the four volatiles are crudely consistent with the abundances in comets (*Mumma and Charnley* 2011). If all the volatiles were in the gas phase, they would have partial pressures of fP_{MMSN}. By comparing the saturation vapor pressures and assumed partial pressures, we find that the snowlines of CO, $\mathrm{CO_2}$, $\mathrm{NH_3}$, and $\mathrm{H_2O}$ are located at $r \approx 206$, 17, 12, and 3.2 au, with sublimation temperatures of ≈ 20, 69, 79, and 156 K, respectively, in this particular disk model (see the circles in Fig. 2). [The abundance of $\mathrm{H_2O}$ relative to $\mathrm{H_2}$ is set to 10^{-3} assuming that $\mathrm{H_2O}$ is the dominant reservoir of oxygen (*Lodders* 2003). If water is mostly inherited from molecular clouds, $\mathrm{H_2O}$ abundance would be 10^{-4} (*Whittet* 1993). Then the water snowline is slightly shifted outwards. We also note that the ices would be a mixture of various molecules, while we consider pure ices here for simplicity. Sublimation of mixed ice is more complicated than that of pure ice (e.g. see review by *Hama and Watanabe* 2013; *Minissale et al.* 2022). For example, laboratory experiments show that the adsorption energy and thus the sublimation temperature of a molecule depends on the composition and surface structure (e.g. crystal or amorphous) of the substrate ice. Referring to the observations of comets and interstellar ice, $\mathrm{H_2O}$ is expected to be a dominant composition of ice in disks. Then a fraction of molecule with higher volatility, such as CO and $\mathrm{CO_2}$, would be trapped in $\mathrm{H_2O}$ ice and desorb at $\mathrm{H_2O}$ snow line.]

The strong dependence of the saturation vapor pressures on temperature illustrated in Fig. 2 clearly indicates that realistic modeling of the disk temperature structure is key to accurately infer the snowline locations. Unfortunately, the simple optically thin disk model adopted above does not apply to protoplanetary disks, which are mostly optically thick to radiation from the central star; in the MMSN, for instance, an optical thickness to stellar radiation can be

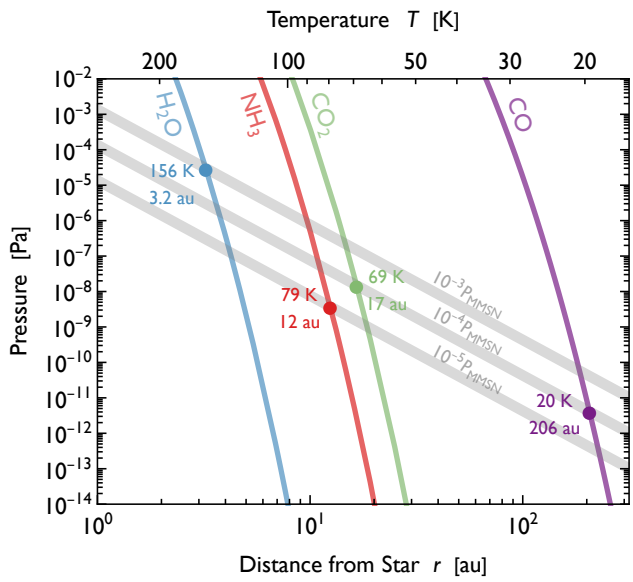

Fig. 2.— Saturation vapor pressures for pure CO, CO_2, NH_3, and H_2O ices (thin lines) as a function of temperature T (indicated on the top edge). For reference, the thick lines show how the temperature and 0.1, 0.01, and 0.001% of the total midplane gas pressure vary with orbital radius (indicated on the bottom edge) in a radially extended version of the classical, optically thin minimum-mass Solar nebula (*Hayashi* 1981). The circles mark the locations of the snowlines.

as high as $\sim 10^5$. Optically thick disks can receive stellar radiation only at their surfaces, and hence their interior temperatures tend to be lower than in optically thin disks unless any internal heat source is present. Specifically, for an optically thick disk passively heated by a central star of luminosity L_* and mass M_*, the temperature of dust grains at the optically thin surface and optically thick midplane can be estimated as (*Kusaka et al.* 1970; *Chiang and Goldreich* 1997)

$$T_{\rm irr,surf} \approx 490 \left(\frac{\epsilon}{0.1}\right)^{-1/4} \left(\frac{L_*}{L_\odot}\right)^{1/4} \left(\frac{r}{1\ {\rm au}}\right)^{-1/2} {\rm K}, \quad (1)$$

$$T_{\rm irr,mid} \approx 120 \left(\frac{L_*}{L_\odot}\right)^{2/7} \left(\frac{M_*}{M_\odot}\right)^{1/7} \left(\frac{r}{1\ {\rm au}}\right)^{-3/7} {\rm K}, \quad (2)$$

respectively, where ϵ is the ratio of the infrared to visible absorption cross sections of the grains at the disk surface. The temperature profile $T_{\rm MMSN}$ of the MMSN disk model is equivalent to $T_{\rm irr,surf}$ with $\epsilon = 1$ and $L_* = 1L_\odot$, where the value $\epsilon = 1$ applies to dust particles larger than microns. We here assume that only submicron-sized grains remain in the surface region and adopt $\epsilon \sim 0.1$ (*Isella and Natta* 2005). The estimate for $T_{\rm irr,mid}$ depends weakly on the height of the surface where the starlight is finally absorbed (*Chiang and Goldreich* 1997). The scale height, and thus $T_{\rm irr,mid}$ depends on the mass of the central star. In Equation (2), we have assumed that the starlight absorption surface lies at three scale heights above the midplane.

The large temperature difference between the midplane and surface regions of the disks has significant implications for the compositional distribution of solids in the disks. Fig. 3(a) illustrates how the locations of the snowlines of some major volatiles at the surface (here referring to three scale heights above the midplane) and at the midplane evolve in an optically thick, passively irradiated disk (see also the snow surface in Fig. 1). Here, the central star is assumed to have a fixed mass of $M_* = 1M_\odot$, while the stellar luminosity is assumed to decrease from $10L_\odot$ at $t = 0.1$ Myr to $0.5L_\odot$ at $t = 10$ Myr in a power-law fashion, mimicking the evolution of solar-mass pre-main-sequence stars. For simplicity, the abundances of the volatiles are assumed to be spatially uniform and equal to the values used in Fig. 2, and the surface density profile of the MMSN is used to calculate the disk pressure distribution. We find from the lower panel of Fig. 3 (a) that the H_2O snowline at the midplane would move inside 1 au—the radius of the current Earth's orbit—within the first million years of star and planet formation. In contrast, the H_2O snowline in the optically thin surface region lies farther away, at more than 10 au from the central star (see the upper panel of Fig. 3 (a)). This difference arises mainly from the vertical temperature (rather than pressure) gradient.

The midplane temperature given by Equation (2) should be taken as a lower limit because we have neglected any internal heat sources. The classical accretion disk model that assumes vertically uniform turbulent viscosity (*Lynden-Bell and Pringle* 1974) predicts that the gravitational energy liberated by mass accretion toward the star can significantly heat the disk interior, in particular in the early disk evolutionary phase where both the accretion rate and disk surface density are high. Fig. 3 (b) illustrates the evolution of the midplane temperature for a disk heated by internal viscous heating in addition to stellar radiation. We consider a solar-mass star and let its luminosity evolve as in Fig. 3 (a). The disk accretion rate is assumed to decay as $\dot{M} = 4\times10^{-8}(t/1\ {\rm Myr})^{-1.07}\ M_\odot\ {\rm yr}^{-1}$ (*Hartmann et al.* 2016). The disk opacity is taken to be $2(T/100\ {\rm K})^2\ {\rm cm}^2\ {\rm g}^{-1}$ (*Bell and Lin* 1994), and the disk's turbulent viscosity is taken to be 1 % of the local sound velocity times the gas scale height. The figure shows that the viscous heating pushes the H_2O snowline out beyond 1 au during the entire Class II phase ($t \lesssim$ several Myr). Note that the temperature evolution illustrated here depends on the disk opacity assumed, and hence on the evolution of dust grains that dominate the opacity. In the disk model adopted here, a factor of 10 decrease in the opacity leads to a factor of $\approx$ two decrease in the midplane temperature.

However, as already mentioned in Sect. 2.1, theoretical studies call into question the applicability of the simple viscous accretion disk model. A more realistic picture of disk accretion may be that the accretion is mainly driven by magnetic fields. In this picture, disk heating still occurs through the Joule dissipation of electric currents associated with the

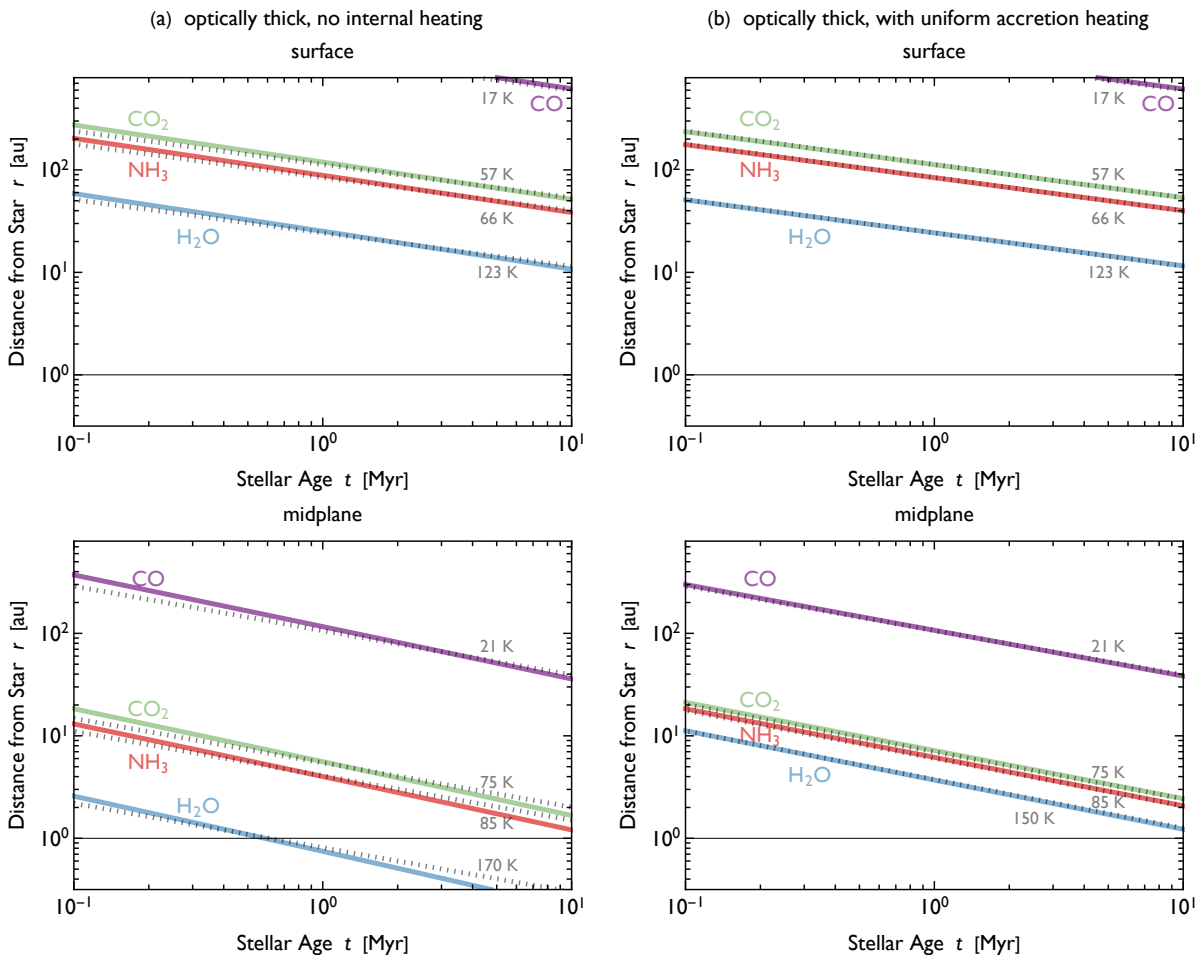

Fig. 3.— Locations of the snowlines for pure CO, CO_2, NH_3, and H_2O ice at the optically thin surface (upper panels) and at the optically thick midplane (lower panels) as a function of stellar age t for disks around a solar-mass pre-main-sequence star. The molar abundances of CO, CO_2, NH_3, and H_2O are assumed to be 10^{-4}, 10^{-4}, 10^{-5}, and 10^{-3}, respectively, everywhere in the disks. Panels (a) are for an optically thick MMSN heated by stellar radiation only, with the snowlines migrating as the stellar luminosity evolves. Panels (b) are for an optically thick, viscous accretion disk with uniform accretion heating in addition to stellar irradiation. In this latter model, the evolution of both the stellar luminosity and accretion rate causes the migration of the snowlines. The dotted lines are contours of constant temperatures, and the thin horizontal line marks the location of the current Earth's orbit, $r = 1$ au.

magnetic fields. However, the Joule heating tends to predominantly occur near the disk surface because the low electric conductivity around the midplane prohibits the development of strong currents. Thermal radiation generated near the surface region can easily escape and is therefore inefficient at heating the midplane region. For this reason, the temperature structure of magnetically accreting disks tends to be close to that of passively irradiated disks as shown in Fig. 3(a) unless both the disk opacity and ionization fraction are sufficiently high (*Hirose and Turner* 2011; *Béthune and Latter* 2020; *Mori et al.* 2019, 2021).

The disk temperature structure and the locations of the snowlines drastically change during episodic accretion outburst events introduced in Sect. 2.1. For example, V883 Ori is a solar-mass FU Ori star with an elevated luminosity of $\sim 200 L_\odot$ (*Furlan et al.* 2016) and a massive circumstellar disk. Equation (2) implies that the midplane of the V883 Ori disk in the outburst phase should be ~ 4.5 times hotter than those of disks around solar-luminosity stars. Assuming a sublimation temperature of 150 K for H_2O ice, we find that the strong irradiation heating should push the H_2O snowline out to $r \sim 20$ au. In reality, the bolometric luminosity of $\sim 200 L_\odot$ includes accretion heating, which could push the snowline further out by heating the disk from inside.

These theoretical estimates of disk temperature structure are compared with SED and spatially-resolved observations of dust continuum and molecular lines. *Cieza et al.* (2016) observed 1.3 mm dust continuum towards V883 Ori to find that the brightness and optical depth sharply rise inward at ~ 40 au. A plausible interpretation is that there is a water snowline at 40 au and ice sublimation causes the

abrupt change of the dust grain size and opacity (see also section 4.2 and *Schoonenberg et al.* 2017). More recently, *Law et al.* (2021b) derived the 2D (radial and vertical) gas temperature distribution of five disks using high- resolution observations ($\sim$ 20 au) of CO and its optically thick isotopologues. The derived temperatures are roughly in agreement with the simple estimates presented in Fig, 3 (see also *Dutrey et al.* 2017; *Flores et al.* 2021).

2.3. Dust growth: theory

In studies of planet formation and protoplanetary disks, dust can refer to any solid particles smaller than planetesimals, not only (sub)micron-sized dust grains but also pebble to boulder-sized solid particles. Although the solids only comprise a minor fraction of the mass in disks, they play significant roles in planet formation and disk evolution. The solids are the ultimate building blocks of all solid bodies in planetary systems including comets. Small dust grains govern the disks' thermal structure, and their size distribution can affect snowline locations (*Oka et al.* 2011) and the disks' hydrodynamical instabilities (*Malygin et al.* 2017; *Barranco et al.* 2018; *Fukuhara et al.* 2021). Thermal emission from micron to millimeter-sized dust particles dominates the disks' continuum emission that we observe with infrared and radio telescopes. Small grains can even regulate the disk MHD by facilitating the recombination of ionized gas particles interacting with magnetic fields (*Sano et al.* 2000; *Ilgner and Nelson* 2006; *Wardle* 2007; *Bai* 2011). Therefore, to understand how solid bodies form in protoplanetary disks, we must fully understand how dust evolves and how it interacts with the disk gas.

From the theoretical point of view, there is no doubt that dust growth starts already in the earliest stage of disk evolution, at least in inner disk regions. Models of dust evolution in both laminar and turbulent disks (*Weidenschilling* 1980; *Nakagawa et al.* 1981; *Dullemond and Dominik* 2005; *Tanaka et al.* 2005; *Brauer et al.* 2008; *Birnstiel et al.* 2010) show that micron-sized grains grow into 0.1–1 mm-sized grains on a timescale of $\ll 1\,\mathrm{Myr}$. In moderately turbulent disks, a useful simple estimate for the local growth timescale (size-doubling time) is available (*Takeuchi et al.* 2005; *Brauer et al.* 2008):

$$t_{\rm grow} \sim \frac{\Sigma_{\rm gas}}{\Sigma_{\rm dust}} \frac{1}{\Omega_{\rm K}} \sim 20 \left(\frac{\Sigma_{\rm gas}/\Sigma_{\rm dust}}{100}\right) \left(\frac{r}{1\,{\rm au}}\right)^{3/2} \left(\frac{M_*}{M_\odot}\right)^{-1/2} \ {\rm yr}, \tag{3}$$

where $\Sigma_{\rm gas}$ and $\Sigma_{\rm dust}$ are the mass surface densities of gas and dust, respectively, and $\Omega_{\rm K}$ is the local Keplerian frequency. Equation (3) does not involve turbulence strength because the negative effect of turbulence on dust settling cancels its positive effect on particle collision speeds. Furthermore, Equation (3) is independent of particle size, implying that the particle radius increases exponentially with time. For instance, micron-sized grains at 30 au would grow to millimeter-sized aggregates in $\sim 2 \times 10^4$ yr. Strictly speaking, Equation (3) overestimates the growth time of small grains that are vertically well mixed in the disk, so the timescale on which millimeter-sized aggregates form can be even shorter. Highly porous (or "fluffy") dust aggregates can also grow faster than estimated by Equation (3) (*Okuzumi et al.* 2012; *Kataoka et al.* 2013; *Garcia and Gonzalez* 2020). In any case, the growth timescale at 30 au is much shorter than the typical ages of Class II disks ($\sim 10^6$ yr) and is even comparable to the ages of the youngest Class 0 sources ($\sim 10^4$ yr).

Equation (3) assumes that grain collisions always result in sticking. This assumption is valid for micron-sized grains with low collisional velocities, unless they are strongly negatively charged in the partially ionized protoplanetary disks (*Okuzumi* 2009). However, as the grain aggregates grow, they obtain a higher collision velocity induced by turbulence (*Ormel and Cuzzi* 2007) and by radial drift on the background gas (*Whipple* 1972; *Adachi et al.* 1976; *Weidenschilling* 1977). The increased collision velocity may prevent further growth by inducing collisional fragmentation (*Blum and Wurm* 2000; *Güttler et al.* 2010) and bouncing (*Güttler et al.* 2010; *Zsom et al.* 2010). Moreover, in a smooth gas disk with a negative radial pressure gradient, their radial drift is inward (see the chapter by Simon et al.). For millimeter and centimeter-sized aggregates, the timescale of the radial inward drift can be shorter than the local growth timescale $t_{\rm grow}$, meaning that these pebbles would fall toward the central star before growing to meter-size boulders. Therefore, a more realistic picture of dust growth is that grains rapidly grow initially and then reach the maximum size set by fragmentation, bouncing, or radial drift (*Birnstiel et al.* 2012; *Drążkowska et al.* 2023). These growth barriers complicate planetesimal formation (see also the chapter by Simon et al.).

In the context of this chapter, it is important to point out that grains' chemical composition is key to understanding how they grow. Early models and experiments suggested that aggregates made of water ice are sticker than silicates (*Dominik and Tielens* 1997) and may even overcome the fragmentation barrier (*Wada et al.* 2009). Such sticky grains also tend to form highly porous aggregates, which is beneficial for overcoming the drift barrier because the porous aggregates grow rapidly (*Okuzumi et al.* 2012; *Kataoka et al.* 2013). However, this sticky water ice scenario is questioned by recent experiments showing that water ice is not so sticky at low temperatures (*Gundlach et al.* 2018; *Musiolik and Wurm* 2019). Instead, some recent studies suggest that silicates are sticker than previously thought (*Kimura et al.* 2015; *Steinpilz et al.* 2019). Some (if not all) types of organic matter are also sticky in a warm environment (*Kouchi et al.* 2002; *Piani et al.* 2017; *Bischoff et al.* 2020). CO_2 ice appears to be less sticky than water ice (*Musiolik et al.* 2016a,b; *Arakawa and Krijt* 2021; *Fritscher and Teiser* 2021). These imply that the fate of dust coagulation and planetesimal formation may depend on temperature and hence on distance from the central star (*Birnstiel et al.* 2010;

Pinilla et al. 2017; *Homma et al.* 2019; *Okuzumi and Tazaki* 2019).

Ice sublimation, condensation, and sintering around snowlines can produce local pileups of solids (*Cuzzi and Zahnle* 2004; *Saito and Sirono* 2011; *Sirono* 2011; *Okuzumi et al.* 2016; *Schoonenberg and Ormel* 2017; *Drążkowska and Alibert* 2017; *Ida and Guillot* 2016; *Ida et al.* 2021; *Hyodo et al.* 2019, 2021). These pileups can have important implications for planetesimal formation and the disks' observational appearance (see also Section 2.5).

2.4. Dust growth: observations

Dust grains are the dominant source of disk opacities. Continuum emission and scattering thus provide information on the physical properties of grains (including size, porosity, and composition). Here, we briefly review important constraints on the degree of dust growth in disks obtained from radio observations. For more comprehensive reviews on disk dust observations, we refer to *Testi et al.* (2014) and *Miotello et al.* (2023).

The spectral index of dust continuum emission in the millimeter wavelength has been used to constrain the maximum grain size in disks; it is defined by

$$\alpha_\nu = \frac{d \ln I_\nu}{d \ln \nu}, \tag{4}$$

where I_ν is the intensity of the emergent radiation at frequency ν. For a black body of uniform temperature T, I_ν is equal to the Planck function $B_\nu(T)$ for the temperature, and one has $\alpha_\nu = 2$ in the Rayleigh–Jeans limit ($B_\nu \propto \nu^2$). For an optically thin disk, one has $I_\nu \approx \kappa_\nu \Sigma_{\rm dust} B_\nu$, where κ_ν is the dust absorption cross section per unit dust mass (*Miyake and Nakagawa* 1993). In the latter case, α_ν reflects the frequency dependence of κ_ν, which in turn reflects the size distribution of opacity-dominating dust grains. For example, interstellar dust grains of maximum size $\sim 0.1\ \mu$m yield $\kappa_\nu \propto \nu^2$ and hence $\alpha_\nu \approx 4$ at radio wavelengths. As the grains grow and their maximum grain size exceeds the wavelengths, the ν dependence of κ_ν becomes weaker, leading to $\alpha_\nu < 4$ (e.g., *Miyake and Nakagawa* 1993). Constraining the grain size from α_ν is also possible for disks that are optically thick but have a non-zero albedo ω_ν, for which $I_\nu \sim \sqrt{1-\omega_\nu} B_\nu$ (*Rybicki and Lightman* 1979). The factor $\sqrt{1-\omega_\nu} (< 1)$ represents the effect of multiple scattering by dust particles in an optically thick disk suppressing the disk's thermal emission (*Rybicki and Lightman* 1979; *Miyake and Nakagawa* 1993; *Birnstiel et al.* 2018; *Liu* 2019; *Zhu et al.* 2019; *Sierra and Lizano* 2020).

Early millimeter and submillimeter surveys (*Weintraub et al.* 1989; *Beckwith et al.* 1990; *Beckwith and Sargent* 1991; *Andrews and Williams* 2005, 2007; *Ricci et al.* 2010a,b) already showed that the spatially integrated continuum emission from T Tauri disks has spectral indices of $\sim$ 2–3 in the (sub)millimeter range. More recently, high-resolution millimeter interferometric observations have provided information on the spatial variation of α_ν in individual disks (*Pérez et al.* 2012, 2015; *ALMA Partnership et al.* 2015; *Guidi et al.* 2016; *Tazzari et al.* 2016; *Huang et al.* 2018; *Cazzoletti et al.* 2018a; *Dent et al.* 2019; *Carrasco-González et al.* 2019; *Soon et al.* 2019; *Macías et al.* 2021). Overall, local values of α_ν range between 1.5–4 and appear to be anticorrelated with millimeter intensity. This anticorrelation indicates either that particles larger than a millimeter are concentrated in the brighter regions or that the brighter regions simply have higher optical depths. In some disks, the spectral index approaches ~ 4 toward the disks' outer edges (*Pérez et al.* 2012; *Guidi et al.* 2016; *Tazzari et al.* 2016; *Dent et al.* 2019; *Carrasco-González et al.* 2019), suggesting that the grains in these outermost regions are smaller than millimeter in size (*Miyake and Nakagawa* 1993). The values of $\alpha_\nu \lesssim 2$ can be explained by optically thick emission from dust grains that have higher albedos at shorter wavelengths. In particular, in the (sub)millimeter wavelength range, $\alpha_\nu \lesssim 2$ implies a population of dust grains with maximum grain sizes of 0.1–1 mm (*Liu* 2019; *Zhu et al.* 2019; *Sierra and Lizano* 2020). An alternative explanation is that the disks with $\alpha_\nu < 2$ have temperatures that decrease with distance from the midplane (*Sierra and Lizano* 2020).

If we assume that the entire disk is optically thin at the observed wavelengths, the spectral index of $\sim$ 2–3 indicates grain growth to millimeters in radius (*Miyake and Nakagawa* 1993; *Draine* 2006). However, it is not evident that the disks, even its outer part, are always optically thin at submillimeter and millimeter wavelengths. Inferring disks' optical thicknesses is intrinsically difficult because the disks' temperature distribution is unknown a priori. *Huang et al.* (2018) and *Dullemond et al.* (2018) used a simple model for the temperature of passively irradiated disks (similar to Equation (2)) and found that some bright dust rings observed in ALMA millimeter images have similar millimeter absorption optical thicknesses of 0.2–1. Although one interpretation is that the rings are barely optically thin by coincidence, another possibility is that the rings are actually optically thick but appear to be darker than the black body because of scattering, $I_\nu \sim \sqrt{1-\omega_\nu} B_\nu$ (*Zhu et al.* 2019).

Recently, radio polarimetric observations have been used to derive independent constraints on the grain size in the outer regions ($\gtrsim$ 10 au) of protoplanetary disks. The observations have shown that many inclined disks produce uniformly polarized submillimeter continuum emission whose polarization direction is parallel to the disks' minor axes (e.g., *Stephens et al.* 2014, 2017; *Hull et al.* 2018; *Harris et al.* 2018; *Cox et al.* 2018; *Sadavoy et al.* 2018; *Dent et al.* 2019). This polarization pattern can be explained if the polarized continuum emission is dust thermal radiation scattered by the dust particles themselves (*Kataoka et al.* 2015; *Yang et al.* 2016). In this interpretation, the observed degree of polarization gives a strong constraint on the size of the opacity-dominating dust particles because the scattering and polarization efficiencies depend strongly on grain size. Models assuming spherical, compact silicate particles (*Kataoka et al.* 2015; *Yang et al.* 2016) predict a maximum

grain size of $\sim 100\ \mu\mathrm{m}$ for the disks with uniformly polarized submillimeter emission.

This new constraint has garnered considerable attention in recent years because the inferred grain size is an order of magnitude smaller than estimated from the spectral index. The cause of the discrepancy between the two grain size estimates is under debate. In fact, the estimates from disk polarized emission largely depend on the grain properties assumed, including grain shape (*Kirchschlager and Bertrang* 2020), porosity (*Tazaki et al.* 2019; *Brunngräber and Wolf* 2021), and composition (*Yang and Li* 2020). For disks that are optically thick at submillimeter wavelengths, the discrepancy may be resolved if grains larger than $\sim 100\ \mu\mathrm{m}$ have already settled to the optically thick midplane region and give no contribution to submillimeter emission, while still affecting the spectral index by contributing to millimeter emission that is optically thinner (*Brunngräber and Wolf* 2020; *Ueda et al.* 2021).

2.5. Dust spatial distribution

With ALMA, we can now observe dust emission from protoplanetary disks in nearby star-forming regions at a spatial resolution of ~ 5 au. Arguably the most striking discovery from the ALMA disk observations is the prevalence of small-scale structures—rings, gaps, spirals, and crescents—in dust thermal emission (e.g., *ALMA Partnership et al.* 2015; *Andrews et al.* 2018; *Long et al.* 2018; *Cieza et al.* 2021). Substructures on similar or smaller scales are also found in near-infrared scattered light images that probe the disk surfaces (e.g., *Avenhaus et al.* 2018; *Garufi et al.* 2018). We refer to *Andrews* (2020) for a review of recent disk substructure observations at both radio and infrared wavelengths.

The most commonly observed substructures are axisymmetric rings and gaps. They were first discovered in the disk around HL Tau (*ALMA Partnership et al.* 2015) and have since been found in many large, bright Class II disks (*Huang et al.* 2018; *Long et al.* 2018). Fig. 4 shows ALMA dust continuum images of the well-studied protoplanetary disks around IM Lup, GM Aur, and AS 209. It illustrates the diversity of the ring/gap substructures: whereas the disk around IM Lup only exhibits shallow gaps (plus spirals), the AS 209 disk features deeper, more extended gaps together with remarkably narrow rings. The disk around GM Aur has a ring connected to a fainter outer disk, a feature also visible in the dust images of some other disks (e.g., Elias 24; *Huang et al.* 2018).

The origins of these dust substructures are a subject of active research (*Andrews* 2020). A widely accepted explanation for narrow dust rings is dust trapping in ring-shape pressure maxima (bumps) (*Pinilla et al.* 2012; *Dullemond et al.* 2018; *Rosotti et al.* 2020), where the radial inward drift of dust particles halts (*Whipple* 1972). This scenario is tempting because dust trapping at pressure bumps has long been anticipated as a solution to the radial drift problem in planetesimal formation (*Johansen et al.* 2014). There are a variety of physical mechanisms potentially yielding annular pressure bumps, including planet–disk interaction (*Paardekooper and Mellema* 2006), MHD effects (*Johansen et al.* 2009; *Suriano et al.* 2018; *Flock et al.* 2015), and dust–gas interaction (*Gonzalez et al.* 2017). Planets can also produce gaps and spirals.

In principle, snowlines could also produce dust rings and gaps as mentioned in Section 2.3. *Zhang et al.* (2015) and *Okuzumi et al.* (2016) argued that the snowlines of major volatiles, including H_2O and CO, are responsible for the major dust rings and gaps in the HL Tau disk. However, the current understanding is that most of the rings and gaps that have been observed in a number of disks are not relevant to snowlines (*Huang et al.* 2018; *Long et al.* 2018; *van der Marel et al.* 2019). The main reason is that the radial positions of the substructures do not appear to be correlated with the central star's luminosity, which should determine snowline locations. Nevertheless, there are a few disks (HD 163296 and MWC 480 in addition to HL Tau) in which a dust ring is found close to the expected location of the CO snowline (*Zhang et al.* 2021).

ALMA observations of dust emission have also provided important constraints on the dust surface density in the outer ($r \gtrsim 10\ \mathrm{au}$) disk region where icy bodies like comets form. If we assume that this region is optically thin to its own millimeter emission, the dust surface density is derived from the millimeter intensity I_ν as $\Sigma_{\mathrm{dust}} = I_\nu/(\kappa_\nu B_\nu)$ (see also Section 2.4). For example, the dust surface densities of the IM Lup, GM Aur, and AS 209 disks are estimated to be comparable or an order of magnitude higher than that in the MMSN (Σ(ice+rock)$= 30(r/1\mathrm{au})^{-3/2}$ g cm^{-2}) for a reasonable assumption about κ_ν for 0.1–1 mm sized grains (see the bottom panels of Fig. 5 in Section 3). We note, however, that these particular objects are among the largest, most massive disks; their dust surface densities may not represent those of more common, compact disks (*Miotello et al.* 2023).

3. Chemistry in Protplanetary disks

Comets contain a significant amount of icy material, which has been investigated to reveal the thermal history and chemical environment in the cold outer regions of the Solar nebula (e.g. chapter by Biver et al.). For example, the composition of major cometary ice is often similar to that of interstellar ice. The relative abundance of CO_2 and CH_3OH to water is $2-30\%$ and $0.2-7\%$ in comets, while these ratios are $15-44\%$ and $5-12\%$ in quiescent molecular clouds (*Mumma and Charnley* 2011). Inheritance of interstellar ice in comets has thus long been discussed. Observations of protoplanetary disks, on the other hand, can reveal the spatial distribution and evolution of molecules at the sites of ongoing planetary-system formation. These two kinds of information are complementary to elucidate the formation of comets and the Solar system.

Theoretical and observational studies show that various chemical processes are going on within the disks (e.g.

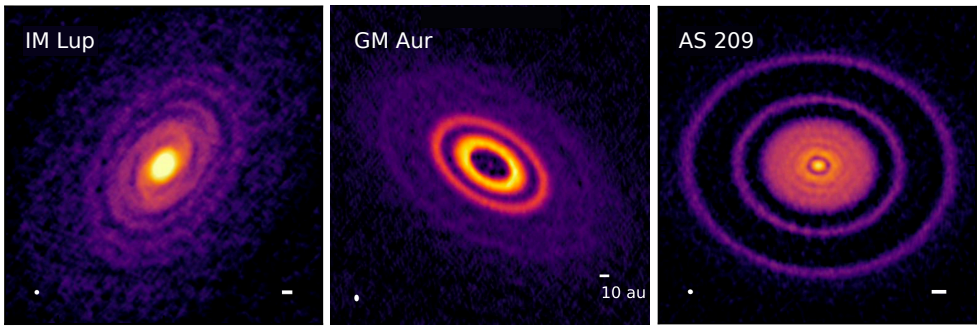

Fig. 4.— ALMA millimeter continuum images of three selected protoplanetary disks (IM Lup and AS 209 adapted from *Andrews et al.* 2018; GM Aur from *Huang et al.* 2020) showing ring/gap substructures in the disks' dust component. Beam sizes and 10 au scale bars are shown in the bottom left and right corners of each panel, respectively. The image of the IM Lup disk also exhibits spirals.

Aikawa et al. 2002; *Henning and Semenov* 2013; *Öberg et al.* 2023). As we have seen in the previous section, there are large gradients of temperature and density in both the radial and vertical directions in a disk (Fig. 1). In the vertical directions, gases are in hydrostatic equilibrium and the density decreases towards the disk surface. The disk surface is directly irradiated by the stellar radiation and thus is warm. Molecules are dissociated to radicals and atoms by UV radiation from the central star [1] and interstellar radiation field; the disk surface is a photon-dominated region (PDR). Beneath the surface layer, there is a warm molecular layer ($\gtrsim$ 20 K), which is moderately shielded from UV radiation and thus harbors various molecular gas such as CO. Ion-molecule reactions are triggered by X-rays from the central object [2] and cosmic rays. In the midplane, the density is highest and dust grains could be further concentrated due to sedimentation. Since the temperature decreases with radial distance, snowlines are defined in the midplane as explained in §2.2 (Fig. 2). Thermal energy could be high enough to drive chemical reactions in the inner hot regions (e.g. above several hundreds of K at < 1 au, *Yang et al.* 2013). Even in the outer cold midplane, reactions in the gas phase and within ices can be triggered by high-energy cosmic rays, X-rays, and decay of radioactive nuclei (e.g. ^{26}Al). Such layered structures, i.e. the PDR layer, warm molecular layer, and icy cold midplane, are confirmed by spatially and spectrally resolved observations (i.e. channel maps) of disks (*Dutrey et al.* 2017; *Ruíz-Rodríguez et al.* 2021; *Rosenfeld et al.* 2013; *Law et al.* 2021b). While the chemical composition of ice in the midplane would be most directly relevant to comets, observation of such ice is not easy (see §3.3). Gaseous line observations in millimeter and submillimeter wavelengths are much more sensitive to low-abundance species. Chemistry in the gas and ice is linked via freeze-out, sublimation, and radial/vertical transport as we will discuss below.

[1] While the surface temperature of T Tauri stars is $\sim$ 4000 K, UV radiation is produced by the gas accretion from the disk to the star.

[2] X-rays are emitted due to magnetic activity on the stellar surface.

In this section, we overview observations of cold molecular gas ($\lesssim$ 100 K) in millimeter and submillimeter wavelengths (§3.1) and warm molecular gas ($\gtrsim$ 100 K) and ice in infrared and shorter wavelengths (§3.2 and §3.3; see also Fig. 1). Table 1 lists the molecular species so far detected in Class II disks in the order of increasing number of atoms and molecular mass. The observed wavelength is listed as well, since it tells where these molecules reside, i.e. cold or warm regions. In addition to the molecular abundances, we cover isotope fractionation and spin temperatures in section §3.4.

3.1. Molecules in cold gas

Fig. 5 shows the radial distributions of the column densities of gaseous molecules and dust grains towards 3 disks around T Tauri stars (IM Lup, GM Aur, and AS 209) derived by ALMA observations (*Öberg et al.* 2021b) with spatial resolutions of $\sim 18 - 48$ au. In the following, we overview what these data tell us about chemistry in disks. Besides the overall chemical structure described above (i.e. the vertically layered structure and snowlines), coupling and decoupling of gas and dust are of special importance, since they could modify not only the molecular abundances but also the local elemental abundances.

3.1.1. CO and H_2O

In molecular clouds, CO and H_2O ice are major Carbon and Oxygen carriers with an abundance of $\sim 10^{-4}$ relative to H_2, and thus are naively expected so in the disks. While H_2O snowlines are too close ($<$ several au) to the central star to be spatially resolved in the observations, CO snowline is at $r \sim 10-30$ au around T Tauri stars (§2.2). The observation of CO snowline is, however, not straightforward, since CO gas is abundant in the warm molecular layer even outside the CO snowline. N_2H^+ line is used to trace the CO snowline; its distribution anti-correlates with CO, since it is destroyed (N_2H^+ + CO $\rightarrow$ N_2 + HCO^+) when CO is abundant in the gas phase (*Qi et al.* 2013a, 2019; *Aikawa et al.* 2015). Alternative tracers are rare isotopes of CO (e.g. $^{13}C^{18}O$), whose emission is expected to be optically

thin (*Zhang et al.* 2017). In TW Hya, for example, the CO snowline is estimated to be $28 - 31$ au and 20.5 au from N_2H^+ and $^{13}C^{18}O$, respectively (*Qi et al.* 2013a; *Zhang et al.* 2017).

The observations of rare isotopes of CO also suggest that the gaseous abundance of CO is actually lower than 10^{-4} even in the warm molecular layer. The CO column densities derived from the observations are compared with the disk models which are constrained by dust continuum emission. As an example, Fig. 5 shows the radial distribution of CO and dust column densities derived from $C^{18}O$ ($J = 2 - 1$) and dust continuum (*Zhang et al.* 2021; *Sierra et al.* 2021). Assuming the gas/dust mass ratio is 100, the CO depletion factor, i.e. the ratio of canonical CO abundance (10^{-4}) divided by the estimated CO abundance in the warm molecular layer, varies from 1 to 100 among disks in radii outside the CO snowline (*Miotello et al.* 2017; *Zhang et al.* 2019, 2021). While the CO abundance tends to increase inwards, the CO depletion factor is $10 - 100$ even inside the CO snowline in some disks. An alternative interpretation of these observations is that the gas/dust mass ratio is lower than 100. The submillimeter HD emission lines, which are observed by *Herschel* towards a limited number of disks, suggest CO depletion rather than gas depletion (*Bergin et al.* 2013; *Favre et al.* 2013; *McClure et al.* 2016). It should however be noted that the evaluation of disk gas mass from HD emission also depends on the assumed thermal structure, i.e. disk models (*Miotello et al.* 2023).

Herschel also observed a few H_2O lines in several disks (*Hogerheijde et al.* 2011; *Salinas et al.* 2016; *Du et al.* 2017). While the beam size (e.g. 37" at 557 GHz) is too large to provide any information on the spatial distribution, the emission lines of H_2O are significantly fainter than the predictions of disk models, in which H_2O is photodesorbed from ice outside its snowline. It suggests that H_2O ice-coated grains are mostly sedimented to the disk midplane where photodesorption is inefficient, and could even be radially drifted inwards (§2.3). The low CO abundance in the warm molecular layer can be explained similarly by the cold-finger effect; while CO is in the gas phase in the warm layer, it could be brought to the cold midplane by weak turbulence to freeze out onto grains. Conversion of CO to less volatile molecules (e.g. CO_2 ice and CH_3OH ice) would also help (e.g. *Furuya and Aikawa* 2014; *Kama et al.* 2016; *Krijt et al.* 2020; *Furuya et al.* 2022a).

It is noteworthy that H_2O ice and CO are expected to be the dominant reservoirs of oxygen and carbon in the initial condition (i.e. gas and solids accreted from the molecular clouds). While both can be depleted from the warm molecular layer as described above, lower volatility of H_2O would result in heavier depletion of oxygen than carbon, and an elemental abundance of C/O > 1 in the warm molecular layer. The high C/O ratio is supported by the observations of other molecules as explained below.

The similarity of the cometary ice with interstellar ice may indicate the sedimentation of ice-coated grains before ice composition is significantly affected by UV and X-rays in the upper layers of the Solar nebula, while molecules formed in the upper layers can still be incorporated into the midplane ice via the cold finger effect.

3.1.2. *Hydrocarbons: C_2H and c-C_3H_2*

Unsaturated hydrocarbons, C_2H and c-C_3H_2, are expected to be abundant in the surface PDR layer, which is supported by the imaging observation of edge-on disks (*Ruíz-Rodríguez et al.* 2021) and their relatively high excitation temperature (20 K $-$ 50 K) (*Guzmán et al.* 2021; *Cleeves et al.* 2021).

The abundance of C_2H is also sensitive to the C/O ratio in the gas phase; the comparison of its line brightness between observations and models indicates C/O > 1 (*Bergin et al.* 2016; *Bergner et al.* 2019; *Miotello et al.* 2019). However, variation among disks should be noted; some disks are faint in C_2H emission (*Miotello et al.* 2019). Spatially resolved observations show that the C_2H emissions often show a ring-like structure. Some rings coincide with the prominent gaps seen in the dust continuum, which is consistent with the expectation that C_2H abundance is enhanced by UV penetration. But not all dust gap correlates with C_2H ring, and vice visa (*Guzmán et al.* 2021; *Law et al.* 2021a).

c-C_3H_2 is detected in several disks, although its emission lines are weaker than those of C_2H (*Qi et al.* 2013b). The column density ratio of c-C_3H_2/C_2H is relatively constant with $5 - 10\%$ in four disks where this ratio is derived (*Ilee et al.* 2021) (Fig. 5). These observations and theoretical models suggest that c-C_3H_2 is formed in the gas phase together with C_2H.

3.1.3. *HCN and CN*

CN is also predicted to be abundant in the surface PDR layer, which is supported by the excitation analysis (*Teague and Loomis* 2020; *Bergner et al.* 2021). A ring-like distribution of CN emission is found in some disks, which is explained by CN formation via the reaction of N atom with UV-pumped vibrationally excited H_2 (*Cazzoletti et al.* 2018b). HCN, on the other hand, is more susceptible to photodissociation than CN; it is dissociated by UV at longer wavelengths than for CN, and by Lyα emitted from T Tauri stars.

A recent high-resolution observation by *Bergner et al.* (2021) show that the column densities of CN and HCN are positively correlated (Fig. 5), which suggests that their formations are connected. For example, chemical models predict that both CN and HCN abundances are enhanced if the C/O ratio is > 1 in the gas phase (*Cleeves et al.* 2018; *Cazzoletti et al.* 2018b). The column density ratio of CN/HCN also increases with radius (Fig. 5), which is consistent with the model prediction that CN is more abundant in the lower density UV-irradiated disk surface (*Bergner et al.* 2021).

3.1.4. *S-bearing molecules*

As in molecular clouds, the abundances of gaseous S-bearing molecules in the disks are much lower than ex-

pected from model predictions assuming the Solar elemental abundance, which suggests significant depletion of sulfur from the gas to the solid phase (see §4.2 and the chapter by Bergin et al.). Six S-bearing molecules are detected in disks: CS, SO, H_2S, H_2CS, C_2S and SO_2. Among them, CS is the most readily detected, and its column density is estimated to be $10^{12} - 10^{13}$ cm^{-2} in several disks (*Le Gal et al.* 2019). Detection of other S-bearing molecules is rather limited. SO is first detected in AB Aur disk by *Fuente et al.* (2010). *Guilloteau et al.* (2016) observed SO in 20 disks using IRAM 30 m and detected the emission only in 4 disks. Prevalence of CS over SO may suggest a high C/O ratio in disks (*Le Gal et al.* 2021). H_2S, the dominant sulfur-bearing molecule in comets, is first detected in disks by *Phuong et al.* (2018), and is recently detected in 4 additional disks (*Rivière-Marichalar et al.* 2021). H_2CS is detected in the disk of Herbig Ae star, MWC 480 (*Le Gal et al.* 2019).

Recently SO_2 was first detected in the disk of IRS 48, which is a transitional disk (i.e. a disk with a central hole in dust continuum emission) with an asymmetric dust emission peak (*Booth et al.* 2021a). The emission peak would correspond to the local pressure maximum, at which dust grains are trapped (§2). Both SO and SO_2 are bright only at this dust peak, while CS is not detected in this disk. The low CS/SO ratio indicates a low C/O ratio (< 1) at the dust trap of IRS 48.

3.1.5. Complex Organic Molecules

In the astrochemistry community, organic molecules consist of 6 atoms and more are called complex organic molecules (COMs). Methanol, the most abundant and prototypical COM in molecular clouds, is so far detected only in TW Hya, HD 100546, IRS 48, and HD 169142 (*Walsh et al.* 2016; *Booth et al.* 2021b; *van der Marel et al.* 2021; *Booth et al.* 2023) in spite of deep searches in some other disks (*Loomis et al.* 2020; *Carney et al.* 2019). It is also the key molecule to investigate the relation between ice and gas in disks; since its formation in the gas phase is known to be inefficient, gaseous CH_3OH should be mainly desorbed from ice, which in turn, is formed by hydrogenation of CO on cold (≤ 20 K) ice surface. The CH_3OH emission in TW Hya is very weak and is in a ring region outside the CO snowline (~ 30 au) and inside the millimeter dust continuum edge. Since the dust temperature in the emitting region is below its sublimation temperature (~ 100 K), CH_3OH is considered to be desorbed by non-thermal processes. HD 100546, on the other hand, is a warm Herbig Ae disk with a central hole in the dust continuum. Most of the CH_3OH emission originates from the spatially unresolved central region (≤ 60 au) and thus could be tracing the thermally sublimated CH_3OH. The warm dust temperature (> 20 K) in the disk of HD 100546 indicates that CH_3OH is not formed in the disk, but inherited from molecular clouds (*Booth et al.* 2021b). In IRS 48, the CH_3OH emission spatially coincides with the dust trap and shows a high excitation temperature ~ 100 K. Gaseous methanol abundance could be enhanced by a combination of ice-coated pebble concentration in the dust trap and irradiation heating at the edge of the central hole (*van der Marel et al.* 2021). Recently, CH_3OCH_3 and CH_3OCHO are also detected at the same position as CH_3OH in IRS 48 (*Brunken et al.* 2022).

Formic acid (HCOOH), which is often detected in the protostellar cores with bright CH_3OH emissions, is so far detected only in TW Hya (*Favre et al.* 2018). H_2CO is another relevant molecule to CH_3OH. It is an intermediate product of CO hydrogenation to form CH_3OH on grain surfaces, while it can be formed via gas-phase reactions as well. H_2CO is also considered to be a precursor species of organics in meteorites (*Cody et al.* 2011). *Pegues et al.* (2020) detected H_2CO in 13 disks out of 15, and derived an excitation temperature of $20 - 50$ K and column density of $\sim 5 \times 10^{11} - 5 \times 10^{14}$ cm^{-2}. The second bottom panels in Fig. 5 show the radial distribution of H_2CO in 3 T Tauri disks assuming the excitation temperature of 20 K (*Guzmán et al.* 2021).

A nitrogen bearing COM, CH_3CN, and another nitrile species HC_3N are detected in several disks (*Öberg et al.* 2015; *Bergner et al.* 2018). *Ilee et al.* (2021) spatially resolved the emission lines of these nitriles in disks of GM Aur, AS 209, HD 163296, and MWC 480; the emission is compact (≤ 100 au) comparable to the extent of the dust continuum. Unlike CH_3OH, these species can be formed in the gas phase. The weak correlation of their emission distributions with the dust continuum, however, may indicate the role of ice reservoir for their formation. The excitation temperatures ($\sim 30 - 50$ K) are lower than their sublimation temperatures, indicating that they are non-thermally desorbed from ice or formed in the gas phase from the species with lower sublimation temperatures. Their column densities ($10^{13} - 10^{14}$ cm^{-2}) (Fig. 5) are higher than predicted in static disk models; either or a combination of grain growth and turbulent mixing would enhance their abundances (*Semenov and Wiebe* 2011; *Furuya and Aikawa* 2014; *Öberg et al.* 2015).

3.2. Molecules in warm and hot gas

Abundant warm molecular gas ($T \gtrsim 200$ K) is generally observed in typical protoplanetary disks surrounding stars of widely different masses (*Brittain et al.* 2003; *Blake and Boogert* 2004; *Brown et al.* 2013). The regions of protoplanetary disks where such warm gas is present are often referred to as the "inner disk". The inner disk may similarly be defined as corresponding to disk radii inside the water snowline. While refractory carbon and silicate-dominated dust sublimate at 1500 K, i.e. at the radius of 0.01-0.1 au for typical protoplanetary disks, many chemically important volatile molecular species (water, CO_2, CH_3OH, CH_4, NH_3, etc.) persist in the gas phase down to dust temperatures of $\sim$100 K or below. Such temperatures are achieved at 1-2 au in the midplane for disks around young solar-mass stars, and at distances of up to $\sim$10 au in the superheated

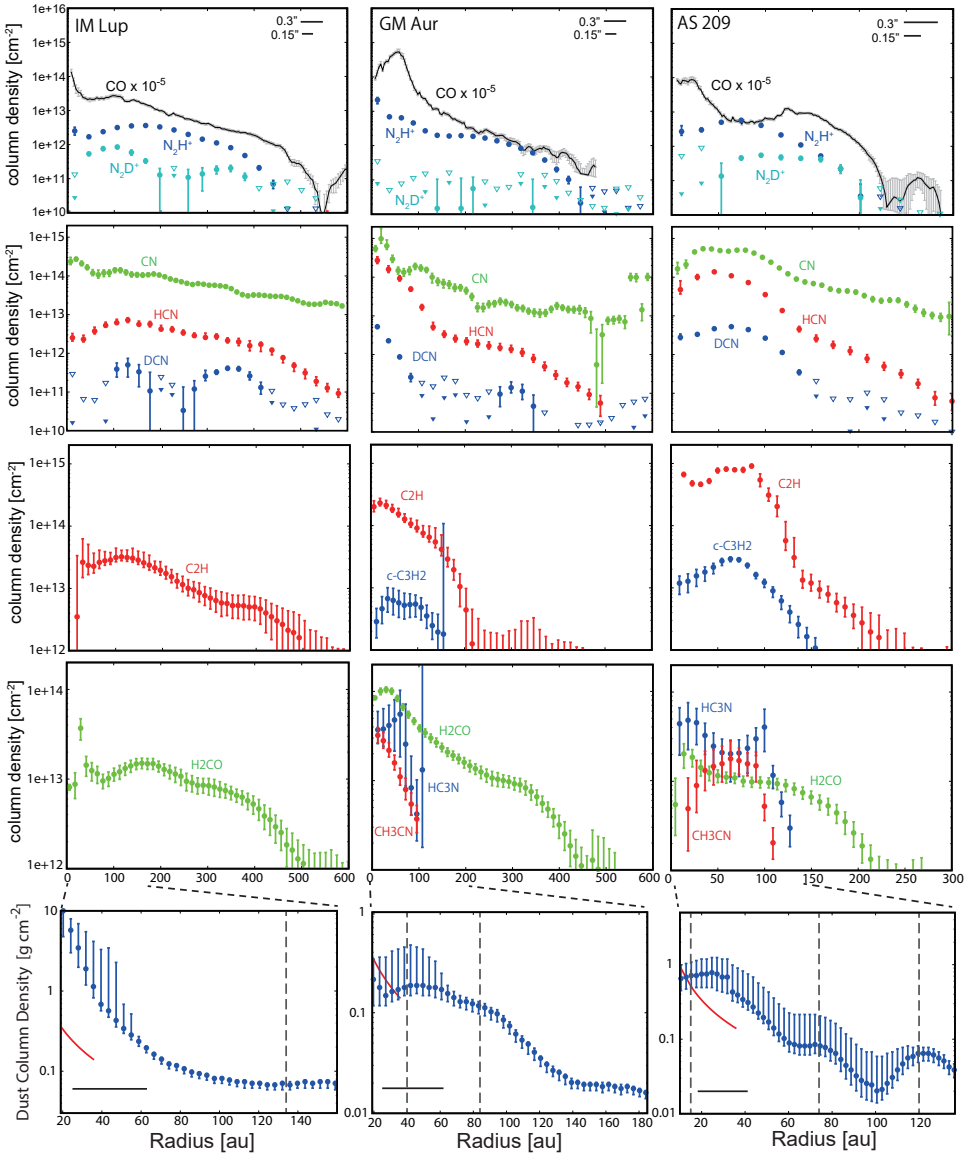

Fig. 5.— Radial column density distributions of gaseous molecules and dust column densities in IM Lup (left), GM Aur (middle), and AS 209 (right) from *Zhang et al.* (2021); *Bergner et al.* (2021); *Cataldi et al.* (2021); *Guzmán et al.* (2021); *Ilee et al.* (2021) and *Sierra et al.* (2021). The molecular column densities of C_2H and CO are derived from the data with a beam size of 0.15", while the beam size is 0.3" for other molecules. The error bars correspond to 1 sigma. For N_2H^+, N_2D^+, and DCN, the 1-sigma and 3-sigma upper limits are plotted at radii where the median value of the molecular column density is lower than the 1-sigma upper limits by a factor of > 10. In the panels of dust column densities, the resolution of the dust continuum observations is shown with a horizontal bar, while the vertical dashed lines depict the positions of the rings. The red curves depict the dust column density of the MMSN (see Section 2.5). .

disk surface (*Sasselov and Lecar* 2000; *Garaud and Lin* 2007) (Fig, 3). Indeed, high-resolution spectroscopy and spectral imaging have demonstrated that the emission originates well inside their respective snowlines (*Goto et al.* 2006; *Pontoppidan et al.* 2008), and that the location of the snowline likely varies with the evolutionary stage of the star-disk system (*Hsieh et al.* 2019, see also §2.2).

Warm molecular gas in disks is readily observed at mid-infrared wavelengths through their ro-vibrational transitions, through high-J pure rotational transitions in the case of water, and in the ultra-violet through electronic transitions (Fig. 6). It is also possible to observe warm and hot gas through rotational transitions between excited vibrational states in the (sub)millimeter regime, but beam dilution of the typically very small emitting inner disk regions makes such lines challenging to detect and image, even with facilities such as ALMA (*Notsu et al.* 2019).

Given the theoretical prediction that the water snow-

line plays a key role in the formation of planets, multiple attempts have been made to observationally measure its location (and that of similar species), but with mixed results. While the CO snowline is located at disk radii large enough to allow for measurements using spatially resolved millimeter interferometric imaging (§3.1.1), the water snowline typically only subtends an angle of 10-100 milli-arcseconds, below the imaging resolution limit of current facilities. Further, while some hot water lines are detectable from the ground, water can only reliably and consistently be detected from space. Consequently, various techniques using purely spectral signatures have been used to constrain the location of the water snowline. *Zhang et al.* (2013) and *Blevins et al.* (2016) used the line spectral energy distribution, representing gas at a range of temperatures, to constrain the water sublimation radius in the surface layer in five protoplanetary disks, finding values of 3-10 au. *Notsu et al.* (2016) proposed a method using optically thin water lines from transitions with low spontaneous emission probability to probe the snowline deeper in the disk, but attempts at detecting the intrinsically weak lines have so far not been successful (*Notsu et al.* 2019).

Because typical protoplanetary disks are primarily externally heated, except for the innermost regions (< 1 au) or disks with very high accretion rates ($> 10^{-7}\, M_{\odot}\, yr^{-1}$) (§2.2), warm molecular gas lines in the infrared overwhelmingly trace the surface layers of the disks (*Kamp and Dullemond* 2004). This effect is exacerbated by the high vertical optical depths of most disks in the 1-10 au radius range. Consequently, the composition of the disk midplanes at these radii is generally not being observed, and can only be inferred under the assumption that some degree of vertical mixing is present (*Semenov and Wiebe* 2011; *Anderson et al.* 2021).

The relative abundances of warm gas-phase volatiles in inner disk surfaces appear to be different from those observed in ices in the cold interstellar medium, and in Solar system comets. This indicates that the observed inner disk chemistry is not directly inherited from cold ice chemistry, but is significantly altered by local processes. Concurrent measurements of H_2 and CO using UV spectroscopy suggest that inner disk CO abundances range from slightly depleted up to canonical ([CO/H_2]$\sim 10^{-5}$–10^{-4}) (*France et al.* 2014; *Cauley et al.* 2021). Other observable species, such as NH_3, CH_4, and CO_2, are further depleted relative to CO by orders of magnitude, clearly inconsistent with primordial ice chemistry (*Mandell et al.* 2012; *Pontoppidan and Blevins* 2014; *Bosman et al.* 2017; *Pontoppidan et al.* 2019b), but consistent with current predictions for warm gas-phase chemistry, which tends to destroy particularly those species, driving nitrogen into N_2 and carbon into CO (*Agúndez et al.* 2008; *Walsh et al.* 2015). Water, on the other hand, is commonly highly abundant in disks around low-mass and solar-mass young stars, as revealed by an extensive sample of disks observed by *Spitzer* (*Carr and Najita* 2008; *Salyk et al.* 2008; *Pontoppidan et al.* 2010; *Carr and Najita* 2011), with retrieved abundances consistent with [CO/H_2O]~ 1 (*Salyk et al.* 2011). JWST is currently confirming the ubiquitous presence of mid-infrared emission from warm gas in inner disks around young stars of all masses, and demonstrate a widening diversity of relative molecular abundances from water and organics (*Tabone et al.* 2023; *Banzatti et al.* 2023; *van Dishoeck et al.* 2023).

3.3. Observations of ices in disks

During most of the evolution of a planetary system, the bulk of its volatile component is sequestered in the solid phase in the form of molecular ices. Indeed, most of the disk mass is typically located beyond the snowline (Fig. 6), with a few notable exceptions such as disks undergoing violent outbursts from instability-induced accretion events, or disks that have been truncated by stellar companions.

While gas-phase volatiles can be relatively easily observed in the warm disk surface, or the hot inner disk inside the snowline, it has proven to be challenging to observe ices in disks, especially in their cold, outer midplanes where the formation of comets is presumably active. Ices are most readily identified through their strong mid-infrared (3-20 μm) resonance bands. However, these bands are nearly universally seen in absorption toward a background source of light, as the dust temperatures required to excite the bands in emission are too high (> 150 K) to retain the ice on the emitting grains. Further, the midplanes of protoplanetary disks during planetesimal formation are generally hidden beneath highly optically thick (at infrared wavelengths) layers of dust.

As a result, direct observations of ices in protoplanetary disks are sparse, and rely on particular geometric configurations that tend to be difficult to interpret. Even in cases where disk ices are detected, such ice is confined to the surface layers of the disk at $\tau_{\rm IR} \sim 1$, corresponding to a fraction of a % of the total vertical column density.

Ices in disks have been observed when the disk is viewed close to edge-on, where ice in a flared outer disk absorbs thermal emission from hot dust in the inner disk, light scattered off the disk surface, or some combination thereof (*Pontoppidan et al.* 2005; *Terada et al.* 2007). Interpretation of such direct absorption spectroscopy is complicated by the complex geometry of the radiative transfer, making it difficult to establish unambiguously the location of the ices within the disk. Further, the signal-to-noise ratios of edge-on disk spectra have often been low due to the inherent faintness of edge-on disks at most infrared wavelengths. In many cases, part of the absorption may also be due to cold material in a remnant protostellar envelope, rather than in the disk itself. In the most unambiguous cases, it appears that the most abundant ices have relative concentrations consistent with those observed in dense clouds and protostellar envelopes (*Aikawa et al.* 2012), although more sensitive observations of rarer species, such as CO_2 and CH_3OH, will likely be needed to establish evolutionary patterns (*Ballering et al.* 2021).

A complementary method for detecting the mid-infrared

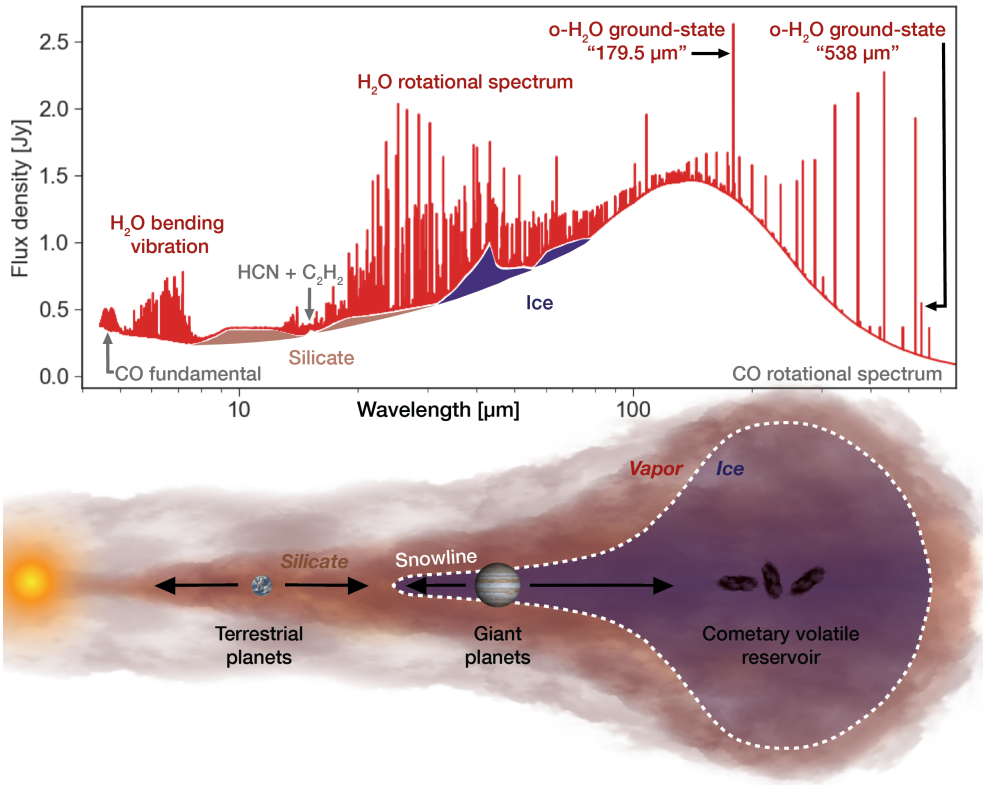

Fig. 6.— Radiative transfer model infrared spectrum of a water-rich protoplanetary disk around a solar-mass star, based on observed *Spitzer* and *Herschel* spectra. The spectrum is rendered at high spectral resolving power ($3\,\mathrm{km\,s^{-1}}$). The spectrum includes lines from CO, water, and organics, and also includes the far-infrared solid-state bands due to water ice at 43 and 62 μm. The figure is reproduced from *Pontoppidan et al.* (2019a).

resonances of ice is through their detection in scattered light. This method is limited for use at the shortest wavelengths where scattering is the most efficient for the grain sizes present in disk surfaces ($< 5\,\mu$m). Thus far, detections of the 3 μm water ice stretching mode have been made in medium-band coronagraphic imaging of a number of face-on disks (*Inoue et al.* 2008; *Honda et al.* 2009, 2016). While clearly demonstrating the presence of ice-coated grains in the uppermost disk surface layers, model fits to ice band optical depths were not able to accurately measure the surface ice/rock ratio, and in particular whether photodesorption is playing a significant role in depleting ice in photo-dominated regions of the disks.

As opposed to the strong mid-infrared ice resonances at 3–15 μm, the far-infrared lattice vibration modes of particularly water ice near 43 and 62 μm (*Warren* 1984; *Hudgins et al.* 1993) appear *in emission* from a significant fraction of the disk dust mass in the comet-forming regions (*Malfait et al.* 1998). The excitation of these features in low-temperature dust means that they are potentially powerful tracers of the ice mass reservoirs. Further, as they are related to vibrations of the solid lattice structure, rather than to vibrations within individual molecules, they are highly sensitive tracers of ice phase and crystallinity. The far-infrared water ice bands have been detected in at least 4 protoplanetary disks, and suggest high abundances of water ice, yielding estimates of ice/rock mass ratios of 0.36-1.6 (*McClure et al.* 2015; *Min et al.* 2016). Attempts have been made to detect far-infrared features in disks from ice species other than water, but these have thus far been unsuccessful, likely due to limitations of sensitivity (*McGuire et al.* 2016; *Giuliano et al.* 2016).

Observations of the molecular inventory in the inner disk may be used to constrain the efficiency of radial transport of ices. *Najita et al.* (2013) found a trend between the mid-infrared HCN/H_2O flux ratio and dust disk mass as measured by ALMA. The proposed interpretation of this apparent link between inner and outer disk properties is that more massive disks may have experienced more efficient build-up of large, water-rich planetesimals, leaving less water ice available in dust grains that migrate inwards. In this case, the observed HCN/H_2O ratio is also a measure of the inner disk elemental C/O ratio. More recently, this scenario was supported by the observation of *Banzatti et al.* (2020), who found a similar relation of enhanced water emission for disks with small dust emission radii, suggesting that compact disks have experienced strong inward radial drift of water-ice rich dust, thereby enriching the inner disk with water vapor and decreasing the local C/O ratio (see also §4.2).

3.4. key markers for comets

3.4.1. Isotope Fractionation

In the Solar system material, isotope ratios of molecules are often different from the elemental abundance ratio. It is called isotope fractionation, and is used to investigate the origin of the planetary material. Isotope ratios in comets and other Solar system materials are reviewed in the chapter by *Biver et al.* (2023). Here we summarize the observations and models of fractionation in disks. We refer *Nomura et al.* (2023) for a more detailed review. There are two mechanisms known to be responsible for the fractionation: (i) exothermic exchange reactions at low temperatures and (ii) selective photodissociation.

The D/H ratio of Earth's ocean (1.56×10^{-4}) is higher than the elemental abundance of D/H in the interstellar matter (1.5×10^{-5}) or the protosolar value (2.1×10^{-5}) (see the chapter by Biver et al. and references therein). Such deuterium fractionation (enrichment) is caused by exchange reactions, e.g.

$$H_3^+ + HD \rightarrow H_2D^+ + H_2 \quad (5)$$

$$CH_3^+ + HD \rightarrow CH_2D^+ + H_2. \quad (6)$$

Since these reactions are exothermic, the backward reactions are inefficient at low temperatures ($\leq$ several 10 K). The high D/H ratio (e.g. H_2D^+/H_3^+) propagates to other molecules via chemical reactions; e.g. HDO is formed by grain surface reactions of O atom or OH with D atom, whose abundance is enhanced by the dissociative recombination of H_2D^+. The high D/H ratio of the ocean suggests that water is supplied to Earth from cold regions, at least partially, and has been motivating the measurement of D/H ratios in comets. The D/H ratio of cometary water, $(1.4-6.5)\times10^{-4}$, overlaps with that of ocean (*Mumma and Charnley* 2011; *Ceccarelli et al.* 2014; *Altwegg et al.* 2015, Chapter by Biver et al.). Recent observations of higher D_2O/HDO ratio than HDO/H_2O both in comet 67P/C-G and protostellar cores indicate the inheritance of comet water from molecular clouds (*Furuya et al.* 2016, 2017; *Altwegg et al.* 2017), while the variation of HDO/H_2O ratio among comets indicates some reprocessing in disks.

In protoplanetary disks, five deuterated molecules, DCO^+, N_2D^+, DCN, C_2D, and HDO are detected so far (e.g. *Huang et al.* 2017; *Salinas et al.* 2017; *Cataldi et al.* 2021; *Öberg et al.* 2021a; *Loomis et al.* 2020; *Tobin et al.* 2023) (Table 1). Disk averaged D/H ratio of the former three species are summarized in Table 2. It should be noted that the recombination timescale of ions is much shorter than the typical ages of disks (i.e. a few 10^6 yr). The high D/H ratio of molecular ions is thus clear evidence of active deuterium fractionation in disks. The D/H ratio of N_2H^+ is higher than that of HCO^+. It is consistent with the theoretical expectation that N_2H^+ traces the cold (< 20 K) layer near the midplane where CO is frozen out, which enhances the deuterium fractionation (*Willacy* 2007; *Cleeves et al.* 2014; *Aikawa et al.* 2015, 2018).

Recently, *Tobin et al.* (2023) detected HDO and $H_2^{18}O$ in the disk of FU Ori star V883 ori, and derived the HDO/H_2O ratio to be $(2.23\pm0.63)\times10^{-3}$. Since this ratio is comparable to those observed in the warm central protostellar cores, they conclude that water in the disk inherit from molecular clouds.

Since temperature increases radially inwards in disks, the molecular D/H ratio is expected to decrease inwards, which is confirmed by the spatially resolved observations of DCN, DCO^+ and N_2D^+ (*Cataldi et al.* 2021; *Öberg et al.* 2021a). The observed peak D/H ratios and their radial positions are summarized in Table 2 (see also Figure 5). The radial distribution of the molecular D/H ratio could also probe the deuteration pathways of each molecular species. The decline of D/H ratio towards the warm central region is expected to be less steep if the molecule is formed mainly via hydrocarbons rather than H_3^+, since the endothermicity of reaction (6) is higher than that of (5) (*Öberg et al.* 2012). *Cataldi et al.* (2021) derived the DCN/HCN ratio as a function of the excitation temperature of HCN (i.e. proxy of gas temperature), which indicates the significant contribution of reaction (6). They also found that the DCN/HCN ratio becomes comparable to the value measured in Hale-Bopp, $(2.3\pm0.4)\times10^{-3}$ (*Meier et al.* 1998; *Crovisier et al.* 2004), in the regions of $\sim 30-40$ K.

The $^{14}N/^{15}N$ ratio of HCN, CN, NH_2 has been measured in comets. The ratio is lower than the elemental abundance in the local interstellar medium ($\sim 200-300$) (e.g. *Ritchey et al.* 2015) and the protosolar value (441) (*Marty et al.* 2011). For example, the average $C^{14}N/C^{15}N$ ratio over 20 comets is 147.8 ± 5.7 (*Manfroid et al.* 2009). The ^{15}N enrichment could be due to exchange reactions and/or selective photodissociation of N_2. The former would be less effective than previously thought, since some key exchange reactions are found to have activation barriers (*Roueff et al.* 2015). In the latter mechanism, $^{14}N^{15}N$ is photodissociated in deeper layers of a disk or molecular cloud than the major isotope, producing excess ^{15}N atoms, which are incorporated to other molecules such as CN (*Liang et al.* 2007; *Heays et al.* 2014; *Furuya et al.* 2017). *Visser et al.* (2018) calculated $^{14}N/^{15}N$ fractionation in disk models to find that the fractionation is fully dominated by selective photodissociation of N_2 (see also *Lee et al.* 2021).

Guzmán et al. (2017) observed $H^{13}CN$ and $HC^{15}N$ to find HCN/$HC^{15}N$ ratio of 80-160 in five disks, which are roughly consistent with the values in comets. In the disk of TW Hya (Table 3), *Hily-Blant et al.* (2019) found that the HCN/$HC^{15}N$ ratio increases with radius, which is consistent with the fractionation due to selective photodissociation (see also *Guzmán et al.* 2017). The ratio of CN/$C^{15}N$, on the other hand, is 323 ± 30 (*Hily-Blant et al.* 2019). The different $^{14}N/^{15}N$ ratio in HCN and CN could be a natural outcome of the vertical gradient of molecular abundance; i.e. CN has its abundance peak in the upper layer than that of HCN (*Cazzoletti et al.* 2018b; *Teague and Loomis* 2020) (§3.1).

Carbon and oxygen isotope ratios in comets are mostly

consistent with the Solar abundance, with the notable exception of some molecules in 67P/C-G (see the chapter by Biver et al. for more details). On the theoretical side, selective photodissociation of CO, combined with isotope exchange reaction of $^{13}C^+ + CO \rightarrow {}^{13}CO + C^+$, could induce fractionation of $^{12}C/^{13}C$ and $^{16}O/^{17}O/^{18}O$ (*Yurimoto and Kuramoto* 2004; *Lyons and Young* 2005). *Miotello et al.* (2014) calculated the isotope fractionation of CO in disk models to show that the abundance and thus the line flux of $C^{18}O$ and $C^{17}O$ could be significantly reduced by the selective photodissociation, especially in disks with grain growth. Observational confirmation is challenging, since the lines of the major isotope of CO are optically thick, while the rare isotope lines are very weak. *Smith et al.* (2009) found that the $C^{18}O/CO$ and $C^{17}O/CO$ ratios are lower than the elemental abundances in the disk of VV CrA by observing absorption lines in the near-infrared with the binary star as a possible light source. As for carbon, *Hily-Blant et al.* (2019) found that the $HCN/H^{13}CN$ ratio is mostly flat with $77.9 - 88.7$ at $R = 20 - 55$ au in the disk of TW Hya. *Yoshida et al.* (2022), on the other hand, derived $^{12}CO/^{13}CO = 21 \pm 5$ at $70 - 110$ au, which indicates the fractionation via the isotope fractionation (C^+ + CO) in the gas of high C/O (> 1) elemental abundance. *Furuya et al.* (2022b) detected $HC^{18}O^+$ emission in TW Hya. Combining this detection with previous $H^{13}CO^+$ observation and disk chemical model, $^{13}CO/C^{18}O$ ratio is estimated to be consistent with the elemental abundance ratio in the local ISM. More recently, *Yamato et al.* (2024b) found that the $^{12}C/^{13}C$ ratios of freshly sublimated complex organic molecules in V883 Ori is low ($\sim 20 - 30$) (section 4.2).

In summary, we see at least a qualitative agreement in deuterium enrichment and nitrogen fractionation between disks and comets, in spite of the fact that we are observing gaseous components in disks, rather than ice.

3.4.2. *Spin Temperature*

Hydrogen atoms have nuclear spin angular momentum, and molecules that contain two or more H atoms in symmetrical locations have quantum states distinguished by the total spin angular momentum (I). In the case of H_2O, for example, $I = 1$ for ortho (o-H_2O) and $I = 0$ for para (p-H_2O). Spontaneous conversion of spin state (e.g. ortho to para) is strongly forbidden by the quantum mechanical selection rules. The rotational energy levels for each spin state form a discrete ladder, and the energy of the lowest-lying level is lower for p-H_2O than o-H_2O by 34.2 K. The relative population of the ortho-to-para ratio (OPR) of H_2O is described as

$$\mathrm{OPR} = \frac{3\Sigma(2J+1)\exp\left(\frac{-E_o(J_{K_a,K_c})}{k_\mathrm{B}T_\mathrm{spin}}\right)}{\Sigma(2J+1)\exp\left(\frac{-E_p(J_{K_a,K_c})}{k_\mathrm{B}T_\mathrm{spin}}\right)}, \qquad (7)$$

where the statistical weight of ortho and para state are 3 and 1, respectively, T_spin is spin temperature, and K_a and K_c are the quantum numbers to describe the projected angular momentum. While the OPR is 3 in the high T_spin limit, the OPR is smaller than 3 due to the energy difference (34.2 K) of the lowest-lying state at < 50 K (*Hama and Watanabe* 2013).

The OPR of H_2O, NH_3, and some other hydrated molecules have been measured in comets, assuming that T_spin is equal to the temperature of the formation site of the molecule (e.g. *Mumma et al.* 1987; *Mumma and Charnley* 2011; *Shinnaka et al.* 2020). The derived spin temperature range is $20 - 60$ K with the typical value of ~ 30 K. For H_2O, the corresponding OPR is ~ 2.5 (*Mumma and Charnley* 2011).

In protoplanetary disks, on the other hand, the OPR of warm water vapor (> 300 K) detected in mid-infrared wavelength is consistent with OPR$= 3$ (*Pontoppidan et al.* 2010; *van Dishoeck et al.* 2013). *Herschel* detected emission lines of cold water vapor (< 100 K) in TW Hya; the OPR is 0.77 ± 0.07, which corresponds to $T_\mathrm{spin} = 13.5 \pm 0.5$ K.

The interpretation of T_spin as the temperature of the molecular formation site, however, turned out to be too simplistic. A laboratory experiment by *Hama et al.* (2018) showed that the OPR of H_2O desorbed from ice is 3 regardless of the temperature of the ice formation (see also *Hama et al.* 2016). While the energy difference of the lowest-lying state between ortho and para is 34.2 K in the gas phase, the rotation motion is constrained and the energy difference becomes significantly small in the ice phase. Then the magnetic dipole interaction of a proton with neighboring protons enables rapid spin conversion (*Limbach et al.* 2006; *Hama et al.* 2018).

The lower OPR than the statistical value observed in comets and outer protoplanetary disks would thus be due to the gas-phase reactions; the spin state changes via proton exchange reactions such as o-$H_2O + H^+ \rightarrow p$-$H_2O + H^+$. The cold water vapor in protoplanetary disks is much less abundant compared with the value expected from the desorption of ice (§3.1). The gas-phase formation of H_2O could thus play a role, while it is much less efficient than the grain-surface reactions at < 20 K. As for comets, the effect of sublimation processes and gas-phase reactions in the coma needs to be considered for the interpretation of the observed OPR ratios (*Hama and Watanabe* 2013; *Hama et al.* 2016)

4. Other Outstanding issues

4.1. From molecular clouds to disks

It has long been discussed whether the molecular composition of volatiles in comets inherits ices in molecular clouds or is reset in the Solar nebula (e.g. *Mumma and Charnley* 2011). To pursue this question, we need to investigate not only Class II disks but also the disk formation stage (i.e. Class 0-I) (section 1). Studies of forming disks have seen significant progress in the last decade.

On the theoretical side, disk formation has been studied by hydrodynamics simulations starting from the collapse of

the parental cloud core, considering the effect of radiation transfer and magnetic fields to derive the physical structures (e.g. size, mass, temperatures) of the disks as a function of time (e.g. *Machida et al.* 2011; *Tsukamoto et al.* 2015; *Hennebelle et al.* 2016; *Tsukamoto et al.* 2023). The molecular evolution of gas and ice is investigated by calculating the chemical reaction network along the gas flow from the cloud core to the disk, considering the temporal variation of density, temperature, and UV radiation flux along the trajectories (e.g. *Visser et al.* 2009, 2011; *Yoneda et al.* 2016; *Drozdovskaya et al.* 2016; *Furuya et al.* 2017; *Aikawa et al.* 2020). Stable abundant ices such as H_2O and CO_2 are delivered to the disk without significant alteration, unless the trajectory is close to the outflow cavity where photodissociation is effective. [Outflows create a cavity (a pair of cone-shaped low-density regions) in the envelope. The wall of the outflow cavity could be irradiated by the UV radiation from the central object.] The abundance of COMs, on the other hand, could increase in the ice mantle as the thermal diffusion and reactions are activated in warm circumstellar conditions (e.g. *Garrod and Herbst* 2006; *Garrod et al.* 2022).

Observations of forming disks are more complicated than those of Class II, since the emission from the disk needs to be distinguished from the infalling envelope and outflow. Careful analysis of spatial distributions and velocity structures shows that emission lines of rare isotopes of CO (with optical depth lower than their normal isotope), H_2CO, and CS tend to probe the disk, while SO traces week accretion shock onto the disk (*Sakai et al.* 2014; *Aso et al.* 2017; *Oya et al.* 2018; *Harsono et al.* 2021; *Tychoniec et al.* 2021; *Garufi et al.* 2021). The vertical stratification of molecules similar to that in Class II disks (§3.1) is also found (*Podio et al.* 2020). *van't Hoff et al.* (2020) show that the young disks tend to be warmer than Class II disks, with the CO snowline at $\geq$ several tens of au, possibly indicating a higher accretion rate (§2.2). Disks with warped structures are also found (e.g. *Sakai et al.* 2019; *Sai et al.* 2020). Recent observations found large-scale (thousands of au) non-axisymmetric steamers onto young disks (*Yen et al.* 2014; *Pineda et al.* 2020; *Garufi et al.* 2022). Such a flow provides chemically fresh interstellar material (e.g. carbon chains) and angular momentum that could perturb the disk structure to enhance mixing.

4.2. Estimation of volatile composition in solids

At the time of writing this review, the direct observations of ices in Class II disks are relatively limited (§3.3), compared with the line observations of gaseous species. Here we overview and discuss how we can estimate the composition and evolution of volatiles in the solid phase based on gaseous observations.

Observations of fresh sublimates are the most straightforward to reveal the ice composition, and are possible during luminosity outbursts. The outbursts, which are caused by a sudden increase of mass accretion from the disk to the central star, are observed in Class I or the transition phase of Class I to Class II (§2.1). While the water snowline is typically located at $\sim$ a few au in Class II disks, it extends further away upon outburst. Around V883 Ori the dust continuum observation suggests that the water snowline is located at $\sim$ 40 au (*Cieza et al.* 2016). V883 Ori is a FU Ori type star, for which the duration of the outburst phase is $\sim$ 100 years. Since it is shorter than typical timescales of the gas-phase chemistry, we can observe fresh sublimates. Various COMs (e.g. CH_3CHO and CH_3OCHO) are detected; their abundances relative to CH_3OH are comparable to those in comets (*Lee et al.* 2019; *Yamato et al.* 2024b). HDO is recently detected as well (Tobin et al., 2023) (section 3.4.1).When the burst ceases, the COMs and water will again freeze on grain surfaces.

As described in §3.1, observations of Class II disks outside the CO snowline indicate that carbon and oxygen are depleted in the warm molecular layer, most probably due to the sedimentation and radial drift of ice-coated dust grains. Observations of molecules such as C_2H suggest a high C/O ratio (> 1) in the gas phase, which in turn suggests that the solid phase is oxygen-rich, e.g. with abundant water ice. The molecular composition of ice could then be determined by the competition of the timescales of dust growth, settling, and molecular evolution in the upper layers of the disk. If the grain growth and settling are fast enough, the ices inherited from molecular clouds might be stored and survive in the midplane, which is cold and shielded from UV and X-ray radiation. Interestingly, recent observations suggest that the growth and sedimentation of dust grains and CO depletion proceed over the short timescale from Class 0/I to II (*Bergner et al.* 2020; *Zhang et al.* 2020; *Harsono et al.* 2021; *Ohashi et al.* 2023).

It should be noted, however, that the freeze-out of gaseous molecules onto grain surfaces continues even after the dust sedimentation. While the turbulence in disks is weaker than previously expected (§2.1), weak turbulence can bring molecules processed in the upper layers to the midplane, where they are frozen onto grains due to low temperature and high density (§3.1). Chemical reactions inside the ice mantle also continue after the sedimentation. For example, impinging cosmic-ray particles cause radiolysis (*Shingledecker et al.* 2018) and/or induce photochemistry (*Gredel et al.* 1989), although the flux of such energy source at the midplane is uncertain (*Cleeves et al.* 2014; *Aikawa et al.* 2021). As the grains migrate to inner radii, the gradual temperature rise enables the thermal diffusion and reactions of radicals inside cracks and pours of the ice mantle. *Krijt et al.* (2020) constructed numerical models that include pebble formation from small dust grains, radial drift of pebbles, diffusion of gas and dust, and simple gas-grain chemistry. They found that the heavy CO depletion observed in several disks is reproduced only in the model with the chemical conversion of CO to less volatile molecules and pebble sedimentation and radial drift. More recently, *Furuya et al.* (2022a) performed calculations with a larger chemical network to show that the depletion of

nitrogen is less severe than that of carbon.

Inside the CO snowline, CO abundance varies among objects (*Zhang et al.* 2019, 2021). In some disks, the CO abundance goes back to the canonical abundance, while it does not in other disks. Assuming that the gas/dust mass ratio is 100, there are two possibilities in the latter case: (i) CO is converted to less volatile species, or (ii) CO ice is locked outside the CO snowline due to the planetesimal formation and/or dust trap at the local pressure maximum. For (i), the product molecules would eventually sublimate when the ice-coated grains reach the inner warmer regions. For (ii), on the other hand, the elemental abundances of carbon and oxygen would be low even in the inner hot regions, ultimately at the inner edge of the disk and in the accreting material from the disk to the central star. *Bosman and Banzatti* (2019) and *McClure et al.* (2020) observed gas at the innermost radius of the TW Hya disk to find that both carbon and oxygen are depleted. This method works for other elements as well. *Kama et al.* (2019) analyzed the stellar spectra of young disk-hosting stars to find depletion of Sulphur, which suggests that $89 \pm 8\%$ of elemental sulfur is in refractory form, e.g. FeS, and trapped in dust traps. The radial variation of elemental abundances should depend on the relative positions of snowlines of major ices and the dust trap or planetesimal formation. Ideally, observations of gases inside the possible comet-forming dust ring could tell us the amount of volatiles used to make comets.

5. Brief summary and future directions

Studies on Solar system material, including comets, and protoplanetary disks play complementary roles in exploring the formation of the Solar system. While comets and asteroids are remnants or fragments of planetesimals, i.e. the building blocks of planetary systems, we can observe their ingredients, i.e. molecules, dust grains, and ices in disks. While the chemical composition of the Solar system material contains rich but degenerated information about their formation environment, the statistical and spatially resolved observations of disks, including those around Class 0 and I objects, reveal the physical and chemical structures and their evolution. Variations of exoplanetary systems suggest that not all disks produce planetary systems like the Solar system. Understanding basic physical and chemical processes in disks is essential to reveal the specific conditions for the Solar system formation.

While ALMA has revealed the thermal emission of dust with sub-arcsecond resolution ($\sim$ 5 au), derivation of the mass distribution of dust grains depends on the opacity, which, in turn, depends on the size distribution of grains. The combination of the observations at various wavelengths, polarization, and theoretical studies on dust properties are crucial (§2). In order to probe the dust in the inner radius, which tends to be optically thick even in millimeter wavelength, low-frequency observations by Band 1 ALMA and ngVLA are essential. These low-frequency instruments are also suited for observations of major volatile molecules such as NH_3 and CH_3OH. In recent years, various ring and linear molecules are newly detected in the line surveys of molecular cloud TMC-1 at Green Bank Telescope and Yabe 40 m telescope at ≤ 50 GHz (*Cernicharo et al.* 2020; *McGuire et al.* 2020). While the detection of new molecules in disks could be limited by sensitivity, since large molecules suitable for low-frequency observations tend to be frozen in ice mantle, disks in outburst could be a good target.

Molecular line observations by ALMA are revealing the gas dynamics (§2), and composition and isotope ratios of disk gas (§3). Theoretical studies of disk chemistry and multi wavelengths observations are crucial to estimate the composition of solids, which is directly linked to comets (§3 and §4). It is clear that a significant fraction of dust grains are grown and decoupled from gas in Class II disks, which makes the elemental abundance heterogeneous. Combined analysis of various molecular lines is important to derive not only the chemical composition but also gas mass distributions in disks. One of the key probes of gas mass is the far-infrared line of HD (§3.1), which would be observable with a new instrument on a suborbital platform, such as a balloon, or a future far-infrared space mission (*Bergin et al.* 2019).

In shorter wavelengths, the James Webb Space Telescope (JWST) is now providing a comprehensive view of inner disk chemistry in protoplanetary disks around stars of a wide range of masses. Active programs include the JWST Disk Infrared Spectroscopic Chemistry Survey (JDISCS, *Pontoppidan et al.* 2024), and the Mid-infrared Disk Survey (MINDS, *Kamp et al.* 2023). These surveys promise to yield inventories of a wide range of bulk volatile species and their isotopologues within the snowline, including water, organics, and nitrogen-bearing species. While the JWST observations will be able to survey disks around stars of all masses, its medium-resolution spectrometer will not be able to spectrally resolve individual lines. However, a new generation of high-resolution spectrometers on ground-based facilities will continue to offer complementary spectroscopy at high resolution. In particular the new CRIRES+ instrument (*Dorn et al.* 2014) on the European Southern Observatory Very Large Telescope (ESO-VLT), and in the future, the METIS instrument (*Brandl et al.* 2010) of the European Extremely Large Telescope and MICHI (*Packham et al.* 2018) on the Thirty Meter Telescope will provide sensitive 3-12 μm spectroscopy of protoplanetary disk chemistry at high spectral and spatial resolution. Finally, the US 2020 Decadal Survey recommended either a far-infrared or X-ray probe class misssion in the 2030s, and several concepts to trace the physics and chemistry of volatiles around the snowline using far-infrared spectroscopy are under consideration (e.g., PRIMA, *Glenn et al.* 2023).

Acknowledgments.
Y.A. acknowledges support by NAOJ ALMA Scientific Research Grant Numbers 2019-13B, Grant-in-Aid for Scientific Research (S) 18H05222, (B) 24K00674, and Grant-in-Aid for Transformative Research Areas (A) 20H05844 and 20H05847. S. O. is supported by JSPS KAKENHI Grant Numbers JP18H05438 and JP20H00182. Part of this work was carried out at the Jet Propulsion Laboratory, California Institute of Technology, under a contract with the National Aeronautics and Space Administration (80NM0018D0004).

REFERENCES

Adachi I., Hayashi C., and Nakazawa K. (1976) *The gas drag effect on the elliptical motion of a solid body in the primordial solar nebula.*, *Progress of Theoretical Physics*, *56*, 1756–1771.

Agúndez M., Cernicharo J., and Goicoechea J. R. (2008) *Formation of simple organic molecules in inner T Tauri disks*, *Astron. Astrophys.*, *483*, 831–837.

Aikawa Y., Cataldi G., Yamato Y. et al. (2021) *Molecules with ALMA at Planet-forming Scales (MAPS). XIII. HCO^+ and Disk Ionization Structure*, *Astrophys. J. Suppl.*, *257*, 13.

Aikawa Y., Furuya K., Hincelin U. et al. (2018) *Multiple Paths of Deuterium Fractionation in Protoplanetary Disks*, *Astrophys. J.*, *855*, 119.

Aikawa Y., Furuya K., Nomura H. et al. (2015) *Analytical Formulae of Molecular Ion Abundances and the N_2H^+ Ring in Protoplanetary Disks*, *Astrophys. J.*, *807*, 120.

Aikawa Y., Furuya K., Yamamoto S. et al. (2020) *Chemical Variation among Protostellar Cores: Dependence on Prestellar Core Conditions*, *Astrophys. J.*, *897*, 110.

Aikawa Y., Kamuro D., Sakon I. et al. (2012) *AKARI observations of ice absorption bands towards edge-on young stellar objects*, *Astron. Astrophys.*, *538*, A57.

Aikawa Y., van Zadelhoff G. J., van Dishoeck E. F. et al. (2002) *Warm molecular layers in protoplanetary disks*, *Astron. Astrophys.*, *386*, 622–632.

ALMA Partnership, Brogan C. L., Pérez L. M. et al. (2015) *The 2014 ALMA Long Baseline Campaign: First Results from High Angular Resolution Observations toward the HL Tau Region*, *Astrophys. J. Lett.*, *808*, L3.

Altwegg K., Balsiger H., Bar-Nun A. et al. (2015) *67P/Churyumov-Gerasimenko, a Jupiter family comet with a high D/H ratio*, *Science*, *347*, 1261952.

Altwegg K., Balsiger H., Berthelier J. J. et al. (2017) *D_2O and HDS in the coma of 67P/Churyumov-Gerasimenko*, *Philosophical Transactions of the Royal Society of London Series A*, *375*, 20160253.

Anderson D. E., Blake G. A., Cleeves L. I. et al. (2021) *Observing Carbon and Oxygen Carriers in Protoplanetary Disks at Mid-infrared Wavelengths*, *Astrophys. J.*, *909*, 55.

Andrews S. M. (2020) *Observations of Protoplanetary Disk Structures*, *Annu. Rev. Astron. Astrophys.*, *58*, 483–528.

Andrews S. M., Huang J., Pérez L. M. et al. (2018) *The Disk Substructures at High Angular Resolution Project (DSHARP). I. Motivation, Sample, Calibration, and Overview*, *Astrophys. J. Lett.*, *869*, L41.

Andrews S. M. and Williams J. P. (2005) *Circumstellar Dust Disks in Taurus-Auriga: The Submillimeter Perspective*, *Astrophys. J.*, *631*, 1134–1160.

Andrews S. M. and Williams J. P. (2007) *A Submillimeter View of Circumstellar Dust Disks in ρ Ophiuchi*, *Astrophys. J.*, *671*, 1800–1812.

Ansdell M., Williams J. P., van der Marel N. et al. (2016) *ALMA Survey of Lupus Protoplanetary Disks. I. Dust and Gas Masses*, *Astrophys. J.*, *828*, 46.

Arakawa S. and Krijt S. (2021) *On the Stickiness of CO_2 and H_2O Ice Particles*, *Astrophys. J.*, *910*, 130.

Arpigny C., Jehin E., Manfroid J. et al. (2003) *Anomalous Nitrogen Isotope Ratio in Comets*, *Science*, *301*, 1522–1525.

Aso Y., Ohashi N., Aikawa Y. et al. (2017) *ALMA Observations of the Protostar L1527 IRS: Probing Details of the Disk and the Envelope Structures*, *Astrophys. J.*, *849*, 56.

Avenhaus H., Quanz S. P., Garufi A. et al. (2018) *Disks around T Tauri Stars with SPHERE (DARTTS-S). I. SPHERE/IRDIS Polarimetric Imaging of Eight Prominent T Tauri Disks*, *Astrophys. J.*, *863*, 44.

Bai X.-N. (2011) *Magnetorotational-instability-driven Accretion in Protoplanetary Disks*, *Astrophys. J.*, *739*, 50.

Bai X.-N. (2013) *Wind-driven Accretion in Protoplanetary Disks. II. Radial Dependence and Global Picture*, *Astrophys. J.*, *772*, 96.

Bai X.-N. (2014) *Hall-effect-Controlled Gas Dynamics in Protoplanetary Disks. I. Wind Solutions at the Inner Disk*, *Astrophys. J.*, *791*, 137.

Bai X.-N. (2017) *Global Simulations of the Inner Regions of Protoplanetary Disks with Comprehensive Disk Microphysics*, *Astrophys. J.*, *845*, 75.

Bai X.-N. and Stone J. M. (2013) *Wind-driven Accretion in Protoplanetary Disks. I. Suppression of the Magnetorotational Instability and Launching of the Magnetocentrifugal Wind*, *Astrophys. J.*, *769*, 76.

Bai X.-N. and Stone J. M. (2017) *Hall Effect-Mediated Magnetic Flux Transport in Protoplanetary Disks*, *Astrophys. J.*, *836*, 46.

Balbus S. A. and Hawley J. F. (1991) *A Powerful Local Shear Instability in Weakly Magnetized Disks. I. Linear Analysis*, *Astrophys. J.*, *376*, 214.

Ballering N. P., Cleeves L. I., and Anderson D. E. (2021) *Simulating Observations of Ices in Protoplanetary Disks*, *Astrophys. J.*, *920*, 115.

Banzatti A., Pascucci I., Bosman A. D. et al. (2020) *Hints for Icy Pebble Migration Feeding an Oxygen-rich Chemistry in the Inner Planet-forming Region of Disks*, *Astrophys. J.*, *903*, 124.

Banzatti A., Pontoppidan K. M., Carr J. S. et al. (2023) *JWST Reveals Excess Cool Water near the Snow Line in Compact Disks, Consistent with Pebble Drift*, *Astrophys. J. Lett.*, *957*, L22.

Barranco J. A., Pei S., and Marcus P. S. (2018) *Zombie Vortex Instability. III. Persistence with Nonuniform Stratification and Radiative Damping*, *Astrophys. J.*, *869*, 127.

Bauer I., Finocchi F., Duschl W. J. et al. (1997) *Simulation of chemical reactions and dust destruction in protoplanetary accretion disks.*, *Astron. Astrophys.*, *317*, 273–289.

Beckwith S. V. W. and Sargent A. I. (1991) *Particle Emissivity in Circumstellar Disks*, *Astrophys. J.*, *381*, 250.

Beckwith S. V. W., Sargent A. I., Chini R. S. et al. (1990) *A Survey for Circumstellar Disks around Young Stellar Objects*, *Astron. J.*, *99*, 924.

Bell K. R. and Lin D. N. C. (1994) *Using FU Orionis Outbursts to Constrain Self-regulated Protostellar Disk Models*, *Astrophys. J.*, *427*, 987.

Bergin E., Pontoppidan K., Bradford C. et al. (2019) *The Disk*

Gas Mass and the Far-IR Revolution, *Bull. Am. Astron. Soc.*, *51*, 222.

Bergin E. A., Cleeves L. I., Gorti U. et al. (2013) *An old disk still capable of forming a planetary system*, *Nature*, *493*, 644–646.

Bergin E. A., Du F., Cleeves L. I. et al. (2016) *Hydrocarbon Emission Rings in Protoplanetary Disks Induced by Dust Evolution*, *Astrophys. J.*, *831*, 101.

Bergner J. B., Guzmán V. G., Öberg K. I. et al. (2018) *A Survey of CH_3CN and HC_3N in Protoplanetary Disks*, *Astrophys. J.*, *857*, 69.

Bergner J. B., Öberg K. I., Bergin E. A. et al. (2020) *An Evolutionary Study of Volatile Chemistry in Protoplanetary Disks*, *Astrophys. J.*, *898*, 97.

Bergner J. B., Öberg K. I., Bergin E. A. et al. (2019) *A Survey of C_2H, HCN, and $C^{18}O$ in Protoplanetary Disks*, *Astrophys. J.*, *876*, 25.

Bergner J. B., Öberg K. I., Guzmán V. V. et al. (2021) *Molecules with ALMA at Planet-forming Scales (MAPS). XI. CN and HCN as Tracers of Photochemistry in Disks*, *Astrophys. J. Suppl.*, *257*, 11.

Béthune W. and Latter H. (2020) *Electric heating and angular momentum transport in laminar models of protoplanetary discs*, *Mon. Not. R. Astron. Soc.*, *494*, 6103–6119.

Birnstiel T., Dullemond C. P., and Brauer F. (2010) *Gas- and dust evolution in protoplanetary disks*, *Astron. Astrophys.*, *513*, A79.

Birnstiel T., Dullemond C. P., Zhu Z. et al. (2018) *The Disk Substructures at High Angular Resolution Project (DSHARP). V. Interpreting ALMA Maps of Protoplanetary Disks in Terms of a Dust Model*, *Astrophys. J. Lett.*, *869*, L45.

Birnstiel T., Klahr H., and Ercolano B. (2012) *A simple model for the evolution of the dust population in protoplanetary disks*, *Astron. Astrophys.*, *539*, A148.

Bischoff D., Kreuzig C., Haack D. et al. (2020) *Sticky or not sticky? Measurements of the tensile strength of microgranular organic materials*, *Mon. Not. R. Astron. Soc.*, *497*, 2517–2528.

Biver N., Dellow Russo N., C. O. et al. (2023) *Chemistry of comet atmosphere*, *COMET III*, *3*, 500–500.

Blake G. A. and Boogert A. C. A. (2004) *High-Resolution 4.7 Micron Keck/NIRSPEC Spectroscopy of the CO Emission from the Disks Surrounding Herbig Ae Stars*, *Astrophys. J. Lett.*, *606*, L73–L76.

Blandford R. D. and Payne D. G. (1982) *Hydromagnetic flows from accretion disks and the production of radio jets.*, *Mon. Not. R. Astron. Soc.*, *199*, 883–903.

Blevins S. M., Pontoppidan K. M., Banzatti A. et al. (2016) *Measurements of Water Surface Snow Lines in Classical Protoplanetary Disks*, *Astrophys. J.*, *818*, 22.

Blum J. and Wurm G. (2000) *Experiments on Sticking, Restructuring, and Fragmentation of Preplanetary Dust Aggregates*, *Icarus*, *143*, 138–146.

Bockelée-Morvan D., Biver N., Jehin E. et al. (2008) *Large Excess of Heavy Nitrogen in Both Hydrogen Cyanide and Cyanogen from Comet 17P/Holmes*, *Astrophys. J. Lett.*, *679*, L49.

Booth A. S., Law C. J., Temmink M. et al. (2023) *Tracing snowlines and C/O ratio in a planet-hosting disk. ALMA molecular line observations towards the HD 169142 disk*, *Astron. Astrophys.*, *678*, A146.

Booth A. S., van der Marel N., Leemker M. et al. (2021a) *A major asymmetric ice trap in a planet-forming disk. II. Prominent SO and SO_2 pointing to C/O < 1*, *Astron. Astrophys.*, *651*, L6.

Booth A. S., Walsh C., Ilee J. D. et al. (2019) *The First Detection of $^{13}C^{17}O$ in a Protoplanetary Disk: A Robust Tracer of Disk Gas Mass*, *Astrophys. J. Lett.*, *882*, L31.

Booth A. S., Walsh C., Kama M. et al. (2018) *Sulphur monoxide exposes a potential molecular disk wind from the planet-hosting disk around HD 100546*, *Astron. Astrophys.*, *611*, A16.

Booth A. S., Walsh C., Terwisscha van Scheltinga J. et al. (2021b) *An inherited complex organic molecule reservoir in a warm planet-hosting disk*, *Nature Astronomy*, *5*, 684–690.

Bosman A. D. and Banzatti A. (2019) *The dry and carbon-poor inner disk of TW Hydrae: evidence for a massive icy dust trap*, *Astron. Astrophys.*, *632*, L10.

Bosman A. D., Bruderer S., and van Dishoeck E. F. (2017) *CO_2 infrared emission as a diagnostic of planet-forming regions of disks*, *Astron. Astrophys.*, *601*, A36.

Brandl B. R., Lenzen R., Pantin E. et al. (2010) in *Ground-based and Airborne Instrumentation for Astronomy III* (I. S. McLean, S. K. Ramsay, and H. Takami, eds.), vol. 7735 of *Society of Photo-Optical Instrumentation Engineers (SPIE) Conference Series*, p. 77352G.

Brauer F., Dullemond C. P., and Henning T. (2008) *Coagulation, fragmentation and radial motion of solid particles in protoplanetary disks*, *Astron. Astrophys.*, *480*, 859–877.

Bridges J. C., Changela H. G., Nayakshin S. et al. (2012) *Chondrule fragments from Comet Wild2: Evidence for high temperature processing in the outer Solar System*, *Earth and Planetary Science Letters*, *341*, 186–194.

Brittain S. D., Rettig T. W., Simon T. et al. (2003) *CO Emission from Disks around AB Aurigae and HD 141569: Implications for Disk Structure and Planet Formation Timescales*, *Astrophys. J.*, *588*, 535–544.

Brown J. M., Pontoppidan K. M., van Dishoeck E. F. et al. (2013) *VLT-CRIRES Survey of Rovibrational CO Emission from Protoplanetary Disks*, *Astrophys. J.*, *770*, 94.

Brunken N. G. C., Booth A. S., Leemker M. et al. (2022) *A major asymmetric ice trap in a planet-forming disk. III. First detection of dimethyl ether*, *Astron. Astrophys.*, *659*, A29.

Brunngräber R. and Wolf S. (2020) *Self-scattering in protoplanetary disks with dust settling*, *Astron. Astrophys.*, *640*, A122.

Brunngräber R. and Wolf S. (2021) *Self-scattering on large, porous grains in protoplanetary disks with dust settling*, *Astron. Astrophys.*, *648*, A87.

Canta A., Teague R., Le Gal R. et al. (2021) *The First Detection of CH_2CN in a Protoplanetary Disk*, *Astrophys. J.*, *922*, 62.

Carney M. T., Hogerheijde M. R., Guzmán V. V. et al. (2019) *Upper limits on CH_3OH in the HD 163296 protoplanetary disk. Evidence for a low gas-phase CH_3OH-to-H_2CO ratio*, *Astron. Astrophys.*, *623*, A124.

Carr J. S. and Najita J. R. (2008) *Organic Molecules and Water in the Planet Formation Region of Young Circumstellar Disks*, *Science*, *319*, 1504.

Carr J. S. and Najita J. R. (2011) *Organic Molecules and Water in the Inner Disks of T Tauri Stars*, *Astrophys. J.*, *733*, 102.

Carr J. S., Tokunaga A. T., and Najita J. (2004) *Hot H_2O Emission and Evidence for Turbulence in the Disk of a Young Star*, *Astrophys. J.*, *603*, 213–220.

Carrasco-González C., Sierra A., Flock M. et al. (2019) *The Radial Distribution of Dust Particles in the HL Tau Disk from ALMA and VLA Observations*, *Astrophys. J.*, *883*, 71.

Cataldi G., Yamato Y., Aikawa Y. et al. (2021) *Molecules with ALMA at Planet-forming Scales (MAPS). X. Studying Deuteration at High Angular Resolution toward Protoplanetary Disks*, *Astrophys. J. Suppl.*, *257*, 10.

Cauley P. W., France K., Herzceg G. J. et al. (2021) *A CO-to-H_2 Ratio of $\sim 10^{-5}$ toward the Herbig Ae Star HK Ori*, *Astron. J.*, *161*, 217.

Cazzoletti P., van Dishoeck E. F., Pinilla P. et al. (2018a) *Evidence for a massive dust-trapping vortex connected to spirals. Multi-wavelength analysis of the HD 135344B protoplanetary disk*, *Astron. Astrophys.*, *619*, A161.

Cazzoletti P., van Dishoeck E. F., Visser R. et al. (2018b) *CN rings in full protoplanetary disks around young stars as probes of disk structure*, *Astron. Astrophys.*, *609*, A93.

Ceccarelli C., Caselli P., Bockelée-Morvan D. et al. (2014) in *Protostars and Planets VI* (H. Beuther, R. S. Klessen, C. P. Dullemond, and T. Henning, eds.), p. 859.

Cernicharo J., Marcelino N., Agúndez M. et al. (2020) *Discovery of HC_4NC in TMC-1: A study of the isomers of HC_3N, HC_5N, and HC_7N*, *Astron. Astrophys.*, *642*, L8.

Chapillon E., Dutrey A., Guilloteau S. et al. (2012) *Chemistry in Disks. VII. First Detection of HC_3N in Protoplanetary Disks*, *Astrophys. J.*, *756*, 58.

Chiang E. I. and Goldreich P. (1997) *Spectral Energy Distributions of T Tauri Stars with Passive Circumstellar Disks*, *Astrophys. J.*, *490*, 368–376.

Cieza L. A., Casassus S., Tobin J. et al. (2016) *Imaging the water snow-line during a protostellar outburst*, *Nature*, *535*, 258–261.

Cieza L. A., González-Ruilova C., Hales A. S. et al. (2021) *The Ophiuchus DIsc Survey Employing ALMA (ODISEA) - III. The evolution of substructures in massive discs at 3-5 au resolution*, *Mon. Not. R. Astron. Soc.*, *501*, 2934–2953.

Cleeves L. I., Bergin E. A., and Adams F. C. (2014) *Exclusion of Cosmic Rays in Protoplanetary Disks. II. Chemical Gradients and Observational Signatures*, *Astrophys. J.*, *794*, 123.

Cleeves L. I., Loomis R. A., Teague R. et al. (2021) *The TW Hya Rosetta Stone Project IV: A Hydrocarbon-rich Disk Atmosphere*, *Astrophys. J.*, *911*, 29.

Cleeves L. I., Öberg K. I., Wilner D. J. et al. (2018) *Constraining Gas-phase Carbon, Oxygen, and Nitrogen in the IM Lup Protoplanetary Disk*, *Astrophys. J.*, *865*, 155.

Cody G. D., Heying E., Alexander C. M. O. et al. (2011) *Cosmochemistry Special Feature: Establishing a molecular relationship between chondritic and cometary organic solids*, *Proceedings of the National Academy of Science*, *108*, 19171–19176.

Connelly J. N., Bizzarro M., Krot A. N. et al. (2012) *The Absolute Chronology and Thermal Processing of Solids in the Solar Protoplanetary Disk*, *Science*, *338*, 651.

Cox E. G., Harris R. J., Looney L. W. et al. (2018) *ALMA's Polarized View of 10 Protostars in the Perseus Molecular Cloud*, *Astrophys. J.*, *855*, 92.

Crovisier J., Bockelée-Morvan D., Colom P. et al. (2004) *The composition of ices in comet C/1995 O1 (Hale-Bopp) from radio spectroscopy. Further results and upper limits on undetected species*, *Astron. Astrophys.*, *418*, 1141–1157.

Cuzzi J. N. and Zahnle K. J. (2004) *Material Enhancement in Protoplanetary Nebulae by Particle Drift through Evaporation Fronts*, *Astrophys. J.*, *614*, 490–496.

Dent W. R. F., Pinte C., Cortes P. C. et al. (2019) *Submillimetre dust polarization and opacity in the HD163296 protoplanetary ring system*, *Mon. Not. R. Astron. Soc.*, *482*, L29–L33.

Desch S. J. and Turner N. J. (2015) *High-temperature Ionization in Protoplanetary Disks*, *Astrophys. J.*, *811*, 156.

Doi K. and Kataoka A. (2021) *Estimate on Dust Scale Height from the ALMA Dust Continuum Image of the HD 163296 Protoplanetary Disk*, *Astrophys. J.*, *912*, 164.

Dominik C. and Tielens A. G. G. M. (1997) *The Physics of Dust Coagulation and the Structure of Dust Aggregates in Space*, *Astrophys. J.*, *480*, 647–673.

Dorn R. J., Anglada-Escude G., Baade D. et al. (2014) *CRIRES+: Exploring the Cold Universe at High Spectral Resolution*, *The Messenger*, *156*, 7–11.

Draine B. T. (2006) *On the Submillimeter Opacity of Protoplanetary Disks*, *Astrophys. J.*, *636*, 1114–1120.

Drążkowska J. and Alibert Y. (2017) *Planetesimal formation starts at the snow line*, *Astron. Astrophys.*, *608*, A92.

Drążkowska J., Bitsch B., Lambrechts M. et al. (2023) in *Protostars and Planets VII* (S. Inutsuka, Y. Aikawa, T. Muto, K. Tomida, and M. Tamura, eds.), vol. 534 of *Astronomical Society of the Pacific Conference Series*, p. 717.

Drozdovskaya M. N., Walsh C., van Dishoeck E. F. et al. (2016) *Cometary ices in forming protoplanetary disc midplanes*, *Mon. Not. R. Astron. Soc.*, *462*, 977–993.

Du F., Bergin E. A., Hogerheijde M. et al. (2017) *Survey of Cold Water Lines in Protoplanetary Disks: Indications of Systematic Volatile Depletion*, *Astrophys. J.*, *842*, 98.

Dullemond C. P., Birnstiel T., Huang J. et al. (2018) *The Disk Substructures at High Angular Resolution Project (DSHARP). VI. Dust Trapping in Thin-ringed Protoplanetary Disks*, *Astrophys. J. Lett.*, *869*, L46.

Dullemond C. P. and Dominik C. (2005) *Dust coagulation in protoplanetary disks: A rapid depletion of small grains*, *Astron. Astrophys.*, *434*, 971–986.

Dutrey A., Guilloteau S., and Guelin M. (1997) *Chemistry of protosolar-like nebulae: The molecular content of the DM Tau and GG Tau disks.*, *Astron. Astrophys.*, *317*, L55–L58.

Dutrey A., Guilloteau S., Piétu V. et al. (2017) *The Flying Saucer: Tomography of the thermal and density gas structure of an edge-on protoplanetary disk*, *Astron. Astrophys.*, *607*, A130.

Evans Neal J. I., Dunham M. M., Jørgensen J. K. et al. (2009) *The Spitzer c2d Legacy Results: Star-Formation Rates and Efficiencies; Evolution and Lifetimes*, *ApJS*, *181*, 321–350.

Favre C., Cleeves L. I., Bergin E. A. et al. (2013) *A Significantly Low CO Abundance toward the TW Hya Protoplanetary Disk: A Path to Active Carbon Chemistry?*, *Astrophys. J. Lett.*, *776*, L38.

Favre C., Fedele D., Semenov D. et al. (2018) *First Detection of the Simplest Organic Acid in a Protoplanetary Disk*, *Astrophys. J. Lett.*, *862*, L2.

Fedele D., Bruderer S., van Dishoeck E. F. et al. (2013) *DIGIT survey of far-infrared lines from protoplanetary disks. I. [O i], [C ii], OH, H_2O, and CH^+*, *Astron. Astrophys.*, *559*, A77.

Fischer W. J., Hillenbrand L. A., Herczeg G. J. et al. (2023) in *Protostars and Planets VII* (S. Inutsuka, Y. Aikawa, T. Muto, K. Tomida, and M. Tamura, eds.), vol. 534 of *Astronomical Society of the Pacific Conference Series*, p. 355.

Flaherty K., Hughes A. M., Simon J. B. et al. (2020) *Measuring Turbulent Motion in Planet-forming Disks with ALMA: A Detection around DM Tau and Nondetections around MWC 480 and V4046 Sgr*, *Astrophys. J.*, *895*, 109.

Flaherty K., Hughes A. M., Simon J. B. et al. (2024) *Evidence for non-zero turbulence in the protoplanetary disc around IM Lup*, *Mon. Not. R. Astron. Soc.*, *532*, 363–380.

Flaherty K. M., Hughes A. M., Rose S. C. et al. (2017) *A Three-dimensional View of Turbulence: Constraints on Turbulent Motions in the HD 163296 Protoplanetary Disk Using DCO^+*, *Astrophys. J.*, *843*, 150.

Flaherty K. M., Hughes A. M., Rosenfeld K. A. et al. (2015) *Weak Turbulence in the HD 163296 Protoplanetary Disk Revealed by ALMA CO Observations*, *Astrophys. J.*, *813*, 99.

Flaherty K. M., Hughes A. M., Teague R. et al. (2018) *Turbulence in the TW Hya Disk*, *Astrophys. J.*, *856*, 117.

Flock M., Ruge J. P., Dzyurkevich N. et al. (2015) *Gaps, rings, and non-axisymmetric structures in protoplanetary disks. From simulations to ALMA observations*, *Astron. Astrophys.*, *574*, A68.

Flock M., Turner N. J., Nelson R. P. et al. (2020) *Gas and Dust Dynamics in Starlight-heated Protoplanetary Disks*, *Astrophys. J.*, *897*, 155.

Flores C., Duchêne G., Wolff S. et al. (2021) *The Anatomy of an Unusual Edge-on Protoplanetary Disk. II. Gas Temperature and a Warm Outer Region*, *Astron. J.*, *161*, 239.

France K., Herczeg G. J., McJunkin M. et al. (2014) *CO/H_2 Abundance Ratio $\approx 10^{-4}$ in a Protoplanetary Disk*, *Astrophys. J.*, *794*, 160.

Fritscher M. and Teiser J. (2021) *CO_2-ice Collisions: A New Experimental Approach*, *Astrophys. J.*, *923*, 134.

Fu R. R., Weiss B. P., Lima E. A. et al. (2014) *Solar nebula magnetic fields recorded in the Semarkona meteorite*, *Science*, *346*, 1089–1092.

Fuente A., Cernicharo J., Agúndez M. et al. (2010) *Molecular content of the circumstellar disk in AB Aurigae. First detection of SO in a circumstellar disk*, *Astron. Astrophys.*, *524*, A19.

Fukuhara Y., Okuzumi S., and Ono T. (2021) *Effects of Dust Evolution on the Vertical Shear Instability in the Outer Regions of Protoplanetary Disks*, *Astrophys. J.*, *914*, 132.

Fung J. and Chiang E. (2016) *Gap Opening in 3D: Single-planet Gaps*, *Astrophys. J.*, *832*, 105.

Furlan E., Fischer W. J., Ali B. et al. (2016) *The Herschel Orion Protostar Survey: Spectral Energy Distributions and Fits Using a Grid of Protostellar Models*, *Astrophys. J. Suppl.*, *224*, 5.

Furuya K. and Aikawa Y. (2014) *Reprocessing of Ices in Turbulent Protoplanetary Disks: Carbon and Nitrogen Chemistry*, *Astrophys. J.*, *790*, 97.

Furuya K., Drozdovskaya M. N., Visser R. et al. (2017) *Water delivery from cores to disks: Deuteration as a probe of the prestellar inheritance of H_2O*, *Astron. Astrophys.*, *599*, A40.

Furuya K., Lee S., and Nomura H. (2022a) *Different Degrees of Nitrogen and Carbon Depletion in the Warm Molecular Layers of Protoplanetary Disks*, *Astrophys. J.*, *938*, 29.

Furuya K., Tsukagoshi T., Qi C. et al. (2022b) *Detection of $HC^{18}O^+$ in a Protoplanetary Disk: Exploring Oxygen Isotope Fractionation of CO*, *Astrophys. J.*, *926*, 148.

Furuya K., van Dishoeck E. F., and Aikawa Y. (2016) *Reconstructing the history of water ice formation from HDO/H_2O and D_2O/HDO ratios in protostellar cores*, *Astron. Astrophys.*, *586*, A127.

Gammie C. F. (1996) *Layered Accretion in T Tauri Disks*, *Astrophys. J.*, *457*, 355.

Garaud P. and Lin D. N. C. (2007) *The Effect of Internal Dissipation and Surface Irradiation on the Structure of Disks and the Location of the Snow Line around Sun-like Stars*, *Astrophys. J.*, *654*, 606–624.

Garcia A. J. L. and Gonzalez J.-F. (2020) *Evolution of porous dust grains in protoplanetary discs - I. Growing grains*, *Mon. Not. R. Astron. Soc.*, *493*, 1788–1800.

Garrod R. T. and Herbst E. (2006) *Formation of methyl formate and other organic species in the warm-up phase of hot molecular cores*, *Astron. Astrophys.*, *457*, 927–936.

Garrod R. T., Jin M., Matis K. A. et al. (2022) *Formation of Complex Organic Molecules in Hot Molecular Cores through Non-diffusive Grain-surface and Ice-mantle Chemistry*, *Astrophys. J. Suppl.*, *259*, 1.

Garufi A., Benisty M., Pinilla P. et al. (2018) *Evolution of protoplanetary disks from their taxonomy in scattered light: spirals, rings, cavities, and shadows*, *Astron. Astrophys.*, *620*, A94.

Garufi A., Podio L., Codella C. et al. (2021) *ALMA chemical survey of disk-outflow sources in Taurus (ALMA-DOT). V. Sample, overview, and demography of disk molecular emission*, *Astron. Astrophys.*, *645*, A145.

Garufi A., Podio L., Codella C. et al. (2022) *ALMA chemical survey of disk-outflow sources in Taurus (ALMA-DOT). VI. Accretion shocks in the disk of DG Tau and HL Tau*, *Astron. Astrophys.*, *658*, A104.

Gibb E. L. and Horne D. (2013) *Detection of CH_4 in the GV Tau N Protoplanetary Disk*, *Astrophys. J. Lett.*, *776*, L28.

Giuliano B. M., Martín-Doménech R., Escribano R. M. et al. (2016) *Interstellar ice analogs: H_2O ice mixtures with CH_3OH and NH_3 in the far-IR region*, *Astron. Astrophys.*, *592*, A81.

Glenn J., Bradford C., Pope A. et al. (2023) in *American Astronomical Society Meeting Abstracts*, vol. 55 of *American Astronomical Society Meeting Abstracts*, p. 160.08.

Gonzalez J. F., Laibe G., and Maddison S. T. (2017) *Self-induced dust traps: overcoming planet formation barriers*, *Mon. Not. R. Astron. Soc.*, *467*, 1984–1996.

Goto M., Usuda T., Dullemond C. P. et al. (2006) *Inner Rim of a Molecular Disk Spatially Resolved in Infrared CO Emission Lines*, *Astrophys. J.*, *652*, 758–762.

Grant S. L., van Dishoeck E. F., Tabone B. et al. (2023) *MINDS. The Detection of $^{13}CO_2$ with JWST-MIRI Indicates Abundant CO_2 in a Protoplanetary Disk*, *Astrophys. J. Lett.*, *947*, L6.

Gredel R., Lepp S., Dalgarno A. et al. (1989) *Cosmic-Ray–induced Photodissociation and Photoionization Rates of Interstellar Molecules*, *Astrophys. J.*, *347*, 289.

Gressel O., Turner N. J., Nelson R. P. et al. (2015) *Global Simulations of Protoplanetary Disks With Ohmic Resistivity and Ambipolar Diffusion*, *Astrophys. J.*, *801*, 84.

Guidi G., Tazzari M., Testi L. et al. (2016) *Dust properties across the CO snowline in the HD 163296 disk from ALMA and VLA observations*, *Astron. Astrophys.*, *588*, A112.

Guilet J. and Ogilvie G. I. (2014) *Global evolution of the magnetic field in a thin disc and its consequences for protoplanetary systems*, *Mon. Not. R. Astron. Soc.*, *441*, 852–868.

Guilloteau S., Di Folco E., Dutrey A. et al. (2013) *A sensitive survey for ^{13}CO, CN, H_2CO, and SO in the disks of T Tauri and Herbig Ae stars*, *Astron. Astrophys.*, *549*, A92.

Guilloteau S., Dutrey A., Wakelam V. et al. (2012) *Chemistry in disks. VIII. The CS molecule as an analytic tracer of turbulence in disks*, *Astron. Astrophys.*, *548*, A70.

Guilloteau S., Reboussin L., Dutrey A. et al. (2016) *Chemistry in disks. X. The molecular content of protoplanetary disks in Taurus*, *Astron. Astrophys.*, *592*, A124.

Gundlach B., Schmidt K. P., Kreuzig C. et al. (2018) *The tensile strength of ice and dust aggregates and its dependence on particle properties*, *Mon. Not. R. Astron. Soc.*, *479*, 1273–1277.

Güttler C., Blum J., Zsom A. et al. (2010) *The outcome of protoplanetary dust growth: pebbles, boulders, or planetesimals?. I. Mapping the zoo of laboratory collision experiments*, *Astron. Astrophys.*, *513*, A56.

Guzmán V. V., Bergner J. B., Law C. J. et al. (2021) *Molecules*

with ALMA at Planet-forming Scales (MAPS). VI. Distribution of the Small Organics HCN, C_2H, and H_2CO, *Astrophys. J. Suppl.*, *257*, 6.

Guzmán V. V., Öberg K. I., Huang J. et al. (2017) *Nitrogen Fractionation in Protoplanetary Disks from the $H^{13}CN/HC^{15}N$ Ratio*, *Astrophys. J.*, *836*, 30.

Hama T., Kouchi A., and Watanabe N. (2016) *Statistical ortho-to-para ratio of water desorbed from ice at 10 kelvin*, *Science*, *351*, 65–67.

Hama T., Kouchi A., and Watanabe N. (2018) *The Ortho-to-para Ratio of Water Molecules Desorbed from Ice Made from Para-water Monomers at 11 K*, *Astrophys. J. Lett.*, *857*, L13.

Hama T. and Watanabe N. (2013) *Surface Processes on Interstellar Amorphous Solid Water: Adsorption, Diffusion, Tunneling Reactions, and Nuclear-Spin Conversion*, *Chemical Reviews*, *113*, 8783–8839.

Harris R. J., Cox E. G., Looney L. W. et al. (2018) *ALMA Observations of Polarized 872 μm Dust Emission from the Protostellar Systems VLA 1623 and L1527*, *Astrophys. J.*, *861*, 91.

Harsono D., van der Wiel M. H. D., Bjerkeli P. et al. (2021) *Resolved molecular line observations reveal an inherited molecular layer in the young disk around TMC1A*, *Astron. Astrophys.*, *646*, A72.

Hartmann L., Herczeg G., and Calvet N. (2016) *Accretion onto Pre-Main-Sequence Stars*, *Annu. Rev. Astron. Astrophys.*, *54*, 135–180.

Hayashi C. (1981) *Structure of the Solar Nebula, Growth and Decay of Magnetic Fields and Effects of Magnetic and Turbulent Viscosities on the Nebula*, *Progress of Theoretical Physics Supplement*, *70*, 35–53.

Heays A. N., Visser R., Gredel R. et al. (2014) *Isotope selective photodissociation of N_2 by the interstellar radiation field and cosmic rays*, *Astron. Astrophys.*, *562*, A61.

Hennebelle P., Commerçon B., Chabrier G. et al. (2016) *Magnetically Self-regulated Formation of Early Protoplanetary Disks*, *Astrophys. J. Lett.*, *830*, L8.

Henning T. and Semenov D. (2013) *Chemistry in Protoplanetary Disks*, *Chemical Reviews*, *113*, 9016–9042.

Hily-Blant P., Magalhaes V., Kastner J. et al. (2017) *Direct evidence of multiple reservoirs of volatile nitrogen in a protosolar nebula analogue*, *Astron. Astrophys.*, *603*, L6.

Hily-Blant P., Magalhaes de Souza V., Kastner J. et al. (2019) *Multiple nitrogen reservoirs in a protoplanetary disk at the epoch of comet and giant planet formation*, *Astron. Astrophys.*, *632*, L12.

Hirose S. and Turner N. J. (2011) *Heating and Cooling Protostellar Disks*, *Astrophys. J. Lett.*, *732*, L30.

Hogerheijde M. R., Bergin E. A., Brinch C. et al. (2011) *Detection of the Water Reservoir in a Forming Planetary System*, *Science*, *334*, 338.

Homma K. A., Okuzumi S., Nakamoto T. et al. (2019) *Rocky Planetesimal Formation Aided by Organics*, *Astrophys. J.*, *877*, 128.

Honda M., Inoue A. K., Fukagawa M. et al. (2009) *Detection of Water Ice Grains on the Surface of the Circumstellar Disk Around HD 142527*, *Astrophys. J. Lett.*, *690*, L110–L113.

Honda M., Kudo T., Takatsuki S. et al. (2016) *Water Ice at the Surface of the HD 100546 Disk*, *Astrophys. J.*, *821*, 2.

Hsieh T.-H., Murillo N. M., Belloche A. et al. (2019) *Chronology of Episodic Accretion in Protostars—An ALMA Survey of the CO and H_2O Snowlines*, *Astrophys. J.*, *884*, 149.

Huang J., Andrews S. M., Dullemond C. P. et al. (2018) *The Disk Substructures at High Angular Resolution Project (DSHARP). II. Characteristics of Annular Substructures*, *Astrophys. J. Lett.*, *869*, L42.

Huang J., Andrews S. M., Dullemond C. P. et al. (2020) *A Multi-frequency ALMA Characterization of Substructures in the GM Aur Protoplanetary Disk*, *Astrophys. J.*, *891*, 48.

Huang J. and Öberg K. I. (2015) *Detection of N_2D^+ in a Protoplanetary Disk*, *Astrophys. J. Lett.*, *809*, L26.

Huang J., Öberg K. I., Qi C. et al. (2017) *An ALMA Survey of $DCN/H^{13}CN$ and $DCO^+/H^{13}CO^+$ in Protoplanetary Disks*, *Astrophys. J.*, *835*, 231.

Hudgins D. M., Sandford S. A., Allamandola L. J. et al. (1993) *Mid- and Far-Infrared Spectroscopy of Ices: Optical Constants and Integrated Absorbances*, *Astrophys. J. Suppl.*, *86*, 713.

Hughes A. M., Wilner D. J., Andrews S. M. et al. (2011) *Empirical Constraints on Turbulence in Protoplanetary Accretion Disks*, *Astrophys. J.*, *727*, 85.

Hull C. L. H., Yang H., Li Z.-Y. et al. (2018) *ALMA Observations of Polarization from Dust Scattering in the IM Lup Protoplanetary Disk*, *Astrophys. J.*, *860*, 82.

Hyodo R., Guillot T., Ida S. et al. (2021) *Planetesimal formation around the snow line. II. Dust or pebbles?*, *Astron. Astrophys.*, *646*, A14.

Hyodo R., Ida S., and Charnoz S. (2019) *Formation of rocky and icy planetesimals inside and outside the snow line: effects of diffusion, sublimation, and back-reaction*, *Astron. Astrophys.*, *629*, A90.

Ida S. and Guillot T. (2016) *Formation of dust-rich planetesimals from sublimated pebbles inside of the snow line*, *Astron. Astrophys.*, *596*, L3.

Ida S., Guillot T., Hyodo R. et al. (2021) *Planetesimal formation around the snow line. I. Monte Carlo simulations of silicate dust pile-up in a turbulent disk*, *Astron. Astrophys.*, *646*, A13.

Ilee J. D., Walsh C., Booth A. S. et al. (2021) *Molecules with ALMA at Planet-forming Scales (MAPS). IX. Distribution and Properties of the Large Organic Molecules HC_3N, CH_3CN, and c-C_3H_2*, *Astrophys. J. Suppl.*, *257*, 9.

Ilgner M. and Nelson R. P. (2006) *On the ionisation fraction in protoplanetary disks. I. Comparing different reaction networks*, *Astron. Astrophys.*, *445*, 205–222.

Inoue A. K., Honda M., Nakamoto T. et al. (2008) *Observational Possibility of the "Snow Line" on the Surface of Circumstellar Disks with the Scattered Light*, *PASJ*, *60*, 557.

Isella A. and Natta A. (2005) *The shape of the inner rim in protoplanetary disks*, *Astron. Astrophys.*, *438*, 899–907.

Johansen A., Blum J., Tanaka H. et al. (2014) in *Protostars and Planets VI* (H. Beuther, R. S. Klessen, C. P. Dullemond, and T. Henning, eds.), p. 547.

Johansen A., Youdin A., and Klahr H. (2009) *Zonal Flows and Long-lived Axisymmetric Pressure Bumps in Magnetorotational Turbulence*, *Astrophys. J.*, *697*, 1269–1289.

Kama M., Bruderer S., van Dishoeck E. F. et al. (2016) *Volatile-carbon locking and release in protoplanetary disks. A study of TW Hya and HD 100546*, *Astron. Astrophys.*, *592*, A83.

Kama M., Shorttle O., Jermyn A. S. et al. (2019) *Abundant Refractory Sulfur in Protoplanetary Disks*, *Astrophys. J.*, *885*, 114.

Kamp I. and Dullemond C. P. (2004) *The Gas Temperature in the Surface Layers of Protoplanetary Disks*, *Astrophys. J.*, *615*, 991–999.

Kamp I., Henning T., Arabhavi A. M. et al. (2023) *The chemical inventory of the inner regions of planet-forming disks – the JWST/MINDS program*, *Faraday Discussions*, *245*, 112–137.

Kataoka A., Muto T., Momose M. et al. (2015) *Millimeter-wave*

Polarization of Protoplanetary Disks due to Dust Scattering, *Astrophys. J.*, *809*, 78.

Kataoka A., Tanaka H., Okuzumi S. et al. (2013) *Fluffy dust forms icy planetesimals by static compression*, *Astron. Astrophys.*, *557*, L4.

Kimura H., Wada K., Senshu H. et al. (2015) *Cohesion of Amorphous Silica Spheres: Toward a Better Understanding of The Coagulation Growth of Silicate Dust Aggregates*, *Astrophys. J.*, *812*, 67.

Kirchschlager F. and Bertrang G. H. M. (2020) *Self-scattering of non-spherical dust grains. The limitations of perfect compact spheres*, *Astron. Astrophys.*, *638*, A116.

Klahr H. and Hubbard A. (2014) *Convective Overstability in Radially Stratified Accretion Disks under Thermal Relaxation*, *Astrophys. J.*, *788*, 21.

Kouchi A., Kudo T., Nakano H. et al. (2002) *Rapid Growth of Asteroids Owing to Very Sticky Interstellar Organic Grains*, *Astrophys. J. Lett.*, *566*, L121–L124.

Krijt S., Bosman A. D., Zhang K. et al. (2020) *CO Depletion in Protoplanetary Disks: A Unified Picture Combining Physical Sequestration and Chemical Processing*, *Astrophys. J.*, *899*, 134.

Kunz M. W. (2008) *On the linear stability of weakly ionized, magnetized planar shear flows*, *Mon. Not. R. Astron. Soc.*, *385*, 1494–1510.

Kusaka T., Nakano T., and Hayashi C. (1970) *Growth of Solid Particles in the Primordial Solar Nebula*, *Progress of Theoretical Physics*, *44*, 1580–1595.

Lahuis F., van Dishoeck E. F., Boogert A. C. A. et al. (2006) *Hot Organic Molecules toward a Young Low-Mass Star: A Look at Inner Disk Chemistry*, *Astrophys. J. Lett.*, *636*, L145–L148.

Law C. J., Loomis R. A., Teague R. et al. (2021a) *Molecules with ALMA at Planet-forming Scales (MAPS). III. Characteristics of Radial Chemical Substructures*, *Astrophys. J. Suppl.*, *257*, 3.

Law C. J., Teague R., Loomis R. A. et al. (2021b) *Molecules with ALMA at Planet-forming Scales (MAPS). IV. Emission Surfaces and Vertical Distribution of Molecules*, *Astrophys. J. Suppl.*, *257*, 4.

Le Gal R., Öberg K. I., Loomis R. A. et al. (2019) *Sulfur Chemistry in Protoplanetary Disks: CS and H_2CS*, *Astrophys. J.*, *876*, 72.

Le Gal R., Öberg K. I., Teague R. et al. (2021) *Molecules with ALMA at Planet-forming Scales (MAPS). XII. Inferring the C/O and S/H Ratios in Protoplanetary Disks with Sulfur Molecules*, *Astrophys. J. Suppl.*, *257*, 12.

Lee J.-E., Lee S., Baek G. et al. (2019) *The ice composition in the disk around V883 Ori revealed by its stellar outburst*, *Nature Astronomy*, *3*, 314–319.

Lee S., Nomura H., Furuya K. et al. (2021) *Modeling Nitrogen Fractionation in the Protoplanetary Disk around TW Hya: Model Constraints on Grain Population and Carbon-to-oxygen Elemental Abundance Ratio*, *Astrophys. J.*, *908*, 82.

Leemker M., Booth A. S., van Dishoeck E. F. et al. (2023) *A major asymmetric ice trap in a planet-forming disk. IV. Nitric oxide gas and a lack of CN tracing sublimating ices and a C/O ratio <1*, *Astron. Astrophys.*, *673*, A7.

Lesur G., Kunz M. W., and Fromang S. (2014) *Thanatology in protoplanetary discs. The combined influence of Ohmic, Hall, and ambipolar diffusion on dead zones*, *Astron. Astrophys.*, *566*, A56.

Leung P. K. C. and Ogilvie G. I. (2019) *Local semi-analytic models of magnetic flux transport in protoplanetary discs*, *Mon. Not. R. Astron. Soc.*, *487*, 5155–5174.

Liang M.-C., Heays A. N., Lewis B. R. et al. (2007) *Source of Nitrogen Isotope Anomaly in HCN in the Atmosphere of Titan*, *Astrophys. J. Lett.*, *664*, L115–L118.

Limbach H.-H., Buntkowsky G., S. G. et al. (2006) *Novel insights into the mechanism of the ortho/para spin conversion of hydrogen pairs: implications for catalysis and interstellar water*, *Chemphyschem*, *7*, 551–4.

Lin D. N. C. and Papaloizou J. C. B. (1993) in *Protostars and Planets III* (E. H. Levy and J. I. Lunine, eds.), p. 749.

Liu H. B. (2019) *The Anomalously Low (Sub)Millimeter Spectral Indices of Some Protoplanetary Disks May Be Explained By Dust Self-scattering*, *Astrophys. J. Lett.*, *877*, L22.

Lodders K. (2003) *Solar System Abundances and Condensation Temperatures of the Elements*, *Astrophys. J.*, *591*, 1220–1247.

Long F., Bosman A. D., Cazzoletti P. et al. (2021) *Exploring HNC and HCN line emission as probes of the protoplanetary disk temperature*, *Astron. Astrophys.*, *647*, A118.

Long F., Pinilla P., Herczeg G. J. et al. (2018) *Gaps and Rings in an ALMA Survey of Disks in the Taurus Star-forming Region*, *Astrophys. J.*, *869*, 17.

Loomis R. A., Öberg K. I., Andrews S. M. et al. (2020) *An Unbiased ALMA Spectral Survey of the LkCa 15 and MWC 480 Protoplanetary Disks*, *Astrophys. J.*, *893*, 101.

Lynden-Bell D. and Pringle J. E. (1974) *The evolution of viscous discs and the origin of the nebular variables.*, *Mon. Not. R. Astron. Soc.*, *168*, 603–637.

Lyons J. R. and Young E. D. (2005) *CO self-shielding as the origin of oxygen isotope anomalies in the early solar nebula*, *Nature*, *435*, 317–320.

Lyra W. (2014) *Convective Overstability in Accretion Disks: Three-dimensional Linear Analysis and Nonlinear Saturation*, *Astrophys. J.*, *789*, 77.

Lyra W. and Umurhan O. M. (2019) *The Initial Conditions for Planet Formation: Turbulence Driven by Hydrodynamical Instabilities in Disks around Young Stars*, *PASP*, *131*, 072001.

Machida M. N., Inutsuka S.-I., and Matsumoto T. (2011) *Effect of Magnetic Braking on Circumstellar Disk Formation in a Strongly Magnetized Cloud*, *PASJ*, *63*, 555.

Macías E., Guerra-Alvarado O., Carrasco-González C. et al. (2021) *Characterizing the dust content of disk substructures in TW Hydrae*, *Astron. Astrophys.*, *648*, A33.

Malfait K., Waelkens C., Waters L. B. F. M. et al. (1998) *The spectrum of the young star HD 100546 observed with the Infrared Space Observatory*, *Astron. Astrophys.*, *332*, L25–L28.

Malygin M. G., Klahr H., Semenov D. et al. (2017) *Efficiency of thermal relaxation by radiative processes in protoplanetary discs: constraints on hydrodynamic turbulence*, *Astron. Astrophys.*, *605*, A30.

Mandell A. M., Bast J., van Dishoeck E. F. et al. (2012) *First Detection of Near-infrared Line Emission from Organics in Young Circumstellar Disks*, *Astrophys. J.*, *747*, 92.

Manfroid J., Jehin E., Hutsemékers D. et al. (2009) *The CN isotopic ratios in comets*, *Astron. Astrophys.*, *503*, 613–624.

Marcus P. S., Pei S., Jiang C.-H. et al. (2015) *Zombie Vortex Instability. I. A Purely Hydrodynamic Instability to Resurrect the Dead Zones of Protoplanetary Disks*, *Astrophys. J.*, *808*, 87.

Martin-Zaïdi C., Lagage P. O., Pantin E. et al. (2007) *Detection of Warm Molecular Hydrogen in the Circumstellar Disk around the Herbig Ae Star HD 97048*, *Astrophys. J. Lett.*, *666*, L117–L120.

Marty B., Chaussidon M., Wiens R. C. et al. (2011) *A ^{15}N-Poor*

Isotopic Composition for the Solar System As Shown by Genesis Solar Wind Samples, *Science*, *332*, 1533.

McClure M. K., Bergin E. A., Cleeves L. I. et al. (2016) *Mass Measurements in Protoplanetary Disks from Hydrogen Deuteride*, *Astrophys. J.*, *831*, 167.

McClure M. K., Dominik C., and Kama M. (2020) *Measuring the atomic composition of planetary building blocks*, *Astron. Astrophys.*, *642*, L15.

McClure M. K., Espaillat C., Calvet N. et al. (2015) *Detections of Trans-Neptunian Ice in Protoplanetary Disks*, *Astrophys. J.*, *799*, 162.

McGuire B. A. (2018) *2018 Census of Interstellar, Circumstellar, Extragalactic, Protoplanetary Disk, and Exoplanetary Molecules*, *Astrophys. J. Suppl.*, *239*, 17.

McGuire B. A., Burkhardt A. M., Loomis R. A. et al. (2020) *Early Science from GOTHAM: Project Overview, Methods, and the Detection of Interstellar Propargyl Cyanide ($HCCCH_2CN$) in TMC-1*, *Astrophys. J. Lett.*, *900*, L10.

McGuire B. A., Ioppolo S., Allodi M. A. et al. (2016) *THz time-domain spectroscopy of mixed CO2-CH3OH interstellar ice analogs*, *Physical Chemistry Chemical Physics (Incorporating Faraday Transactions)*, *18*, 20199–20207.

Meier R., Owen T. C., Jewitt D. C. et al. (1998) *Deuterium in Comet C/1995 O1 (Hale-Bopp): Detection of DCN*, *Science*, *279*, 1707.

Min M., Bouwman J., Dominik C. et al. (2016) *The abundance and thermal history of water ice in the disk surrounding HD 142527 from the DIGIT Herschel Key Program*, *Astron. Astrophys.*, *593*, A11.

Minissale M., Aikawa Y., Bergin E. et al. (2022) *Thermal Desorption of Interstellar Ices: A Review on the Controlling Parameters and Their Implications from Snowlines to Chemical Complexity*, *ACS Earth and Space Chemistry*, *6*, 597–630.

Miotello A., Bruderer S., and van Dishoeck E. F. (2014) *Protoplanetary disk masses from CO isotopologue line emission*, *Astron. Astrophys.*, *572*, A96.

Miotello A., Facchini S., van Dishoeck E. F. et al. (2019) *Bright C_2H emission in protoplanetary discs in Lupus: high volatile $C/O > 1$ ratios*, *Astron. Astrophys.*, *631*, A69.

Miotello A., Kamp I., Birnstiel T. et al. (2023) in *Protostars and Planets VII* (S. Inutsuka, Y. Aikawa, T. Muto, K. Tomida, and M. Tamura, eds.), vol. 534 of *Astronomical Society of the Pacific Conference Series*, p. 501.

Miotello A., van Dishoeck E. F., Williams J. P. et al. (2017) *Lupus disks with faint CO isotopologues: low gas/dust or high carbon depletion?*, *Astron. Astrophys.*, *599*, A113.

Miyake K. and Nakagawa Y. (1993) *Effects of Particle Size Distribution on Opacity Curves of Protoplanetary Disks around T Tauri Stars*, *Icarus*, *106*, 20–41.

Morbidelli A., Szulágyi J., Crida A. et al. (2014) *Meridional circulation of gas into gaps opened by giant planets in three-dimensional low-viscosity disks*, *Icarus*, *232*, 266–270.

Mori S., Bai X.-N., and Okuzumi S. (2019) *Temperature Structure in the Inner Regions of Protoplanetary Disks: Inefficient Accretion Heating Controlled by Nonideal Magnetohydrodynamics*, *Astrophys. J.*, *872*, 98.

Mori S., Okuzumi S., Kunitomo M. et al. (2021) *Evolution of the Water Snow Line in Magnetically Accreting Protoplanetary Disks*, *Astrophys. J.*, *916*, 72.

Mumma M. J. and Charnley S. B. (2011) *The Chemical Composition of Comets—Emerging Taxonomies and Natal Heritage*, *Annu. Rev. Astron. Astrophys.*, *49*, 471–524.

Mumma M. J., Weaver H. A., and Larson H. P. (1987) *The Ortho-Para Ratio of Water Vapor in Comet p/ Halley*, *Astron. Astrophys.*, *187*, 419.

Musiolik G., Teiser J., Jankowski T. et al. (2016a) *Collisions of CO_2 Ice Grains in Planet Formation*, *Astrophys. J.*, *818*, 16.

Musiolik G., Teiser J., Jankowski T. et al. (2016b) *Ice Grain Collisions in Comparison: CO2, H2O, and Their Mixtures*, *Astrophys. J.*, *827*, 63.

Musiolik G. and Wurm G. (2019) *Contacts of Water Ice in Protoplanetary Disks—Laboratory Experiments*, *Astrophys. J.*, *873*, 58.

Najita J., Carr J. S., and Mathieu R. D. (2003) *Gas in the Terrestrial Planet Region of Disks: CO Fundamental Emission from T Tauri Stars*, *Astrophys. J.*, *589*, 931–952.

Najita J. R., Carr J. S., Brittain S. D. et al. (2021) *High-resolution Mid-infrared Spectroscopy of GV Tau N: Surface Accretion and Detection of NH_3 in a Young Protoplanetary Disk*, *Astrophys. J.*, *908*, 171.

Najita J. R., Carr J. S., Pontoppidan K. M. et al. (2013) *The HCN-Water Ratio in the Planet Formation Region of Disks*, *Astrophys. J.*, *766*, 134.

Nakagawa Y., Nakazawa K., and Hayashi C. (1981) *Growth and sedimentation of dust grains in the primordial solar nebula*, *Icarus*, *45*, 517–528.

Nelson R. P., Gressel O., and Umurhan O. M. (2013) *Linear and non-linear evolution of the vertical shear instability in accretion discs*, *Mon. Not. R. Astron. Soc.*, *435*, 2610–2632.

Nomura H., Furuya K., Cordiner M. A. et al. (2023) in *Astronomical Society of the Pacific Conference Series* (S. Inutsuka, Y. Aikawa, T. Muto, K. Tomida, and M. Tamura, eds.), vol. 534 of *Astronomical Society of the Pacific Conference Series*, p. 1075.

Notsu S., Akiyama E., Booth A. et al. (2019) *Dust Continuum Emission and the Upper Limit Fluxes of Submillimeter Water Lines of the Protoplanetary Disk around HD 163296 Observed by ALMA*, *Astrophys. J.*, *875*, 96.

Notsu S., Nomura H., Ishimoto D. et al. (2016) *Candidate Water Vapor Lines to Locate the H2O Snowline through High-dispersion Spectroscopic Observations. I. The Case of a T Tauri Star*, *Astrophys. J.*, *827*, 113.

Öberg K. I., Cleeves L. I., Bergner J. B. et al. (2021a) *The TW Hya Rosetta Stone Project. I. Radial and Vertical Distributions of DCN and DCO^+*, *Astron. J.*, *161*, 38.

Öberg K. I., Facchini S., and Anderson D. E. (2023) *Protoplanetary Disk Chemistry*, *Annu. Rev. Astron. Astrophys.*, *61*, 287–328.

Öberg K. I., Guzmán V. V., Furuya K. et al. (2015) *The comet-like composition of a protoplanetary disk as revealed by complex cyanides*, *Nature*, *520*, 198–201.

Öberg K. I., Guzmán V. V., Walsh C. et al. (2021b) *Molecules with ALMA at Planet-forming Scales (MAPS). I. Program Overview and Highlights*, *Astrophys. J. Suppl.*, *257*, 1.

Öberg K. I., Murray-Clay R., and Bergin E. A. (2011) *The Effects of Snowlines on C/O in Planetary Atmospheres*, *Astrophys. J. Lett.*, *743*, L16.

Öberg K. I., Qi C., Wilner D. J. et al. (2012) *Evidence for Multiple Pathways to Deuterium Enhancements in Protoplanetary Disks*, *Astrophys. J.*, *749*, 162.

Offner S. S. R. and McKee C. F. (2011) *The Protostellar Luminosity Function*, *Astrophys. J.*, *736*, 53.

Ohashi N., Tobin J. J., Jørgensen J. K. et al. (2023) *Early Planet Formation in Embedded Disks (eDisk). I. Overview of the Pro-*

gram and First Results, *Astrophys. J.*, *951*, 8.

Oka A., Nakamoto T., and Ida S. (2011) *Evolution of Snow Line in Optically Thick Protoplanetary Disks: Effects of Water Ice Opacity and Dust Grain Size*, *Astrophys. J.*, *738*, 141.

Okuzumi S. (2009) *Electric Charging of Dust Aggregates and its Effect on Dust Coagulation in Protoplanetary Disks*, *Astrophys. J.*, *698*, 1122–1135.

Okuzumi S., Momose M., Sirono S.-i. et al. (2016) *Sintering-induced Dust Ring Formation in Protoplanetary Disks: Application to the HL Tau Disk*, *Astrophys. J.*, *821*, 82.

Okuzumi S., Takeuchi T., and Muto T. (2014) *Radial Transport of Large-scale Magnetic Fields in Accretion Disks. I. Steady Solutions and an Upper Limit on the Vertical Field Strength*, *Astrophys. J.*, *785*, 127.

Okuzumi S., Tanaka H., Kobayashi H. et al. (2012) *Rapid Coagulation of Porous Dust Aggregates outside the Snow Line: A Pathway to Successful Icy Planetesimal Formation*, *Astrophys. J.*, *752*, 106.

Okuzumi S. and Tazaki R. (2019) *Nonsticky Ice at the Origin of the Uniformly Polarized Submillimeter Emission from the HL Tau Disk*, *Astrophys. J.*, *878*, 132.

Ormel C. W. and Cuzzi J. N. (2007) *Closed-form expressions for particle relative velocities induced by turbulence*, *Astron. Astrophys.*, *466*, 413–420.

Oya Y., Moriwaki K., Onishi S. et al. (2018) *Chemical and Physical Picture of IRAS 16293-2422 Source B at a Sub-arcsecond Scale Studied with ALMA*, *Astrophys. J.*, *854*, 96.

Paardekooper S. J. and Mellema G. (2006) *Dust flow in gas disks in the presence of embedded planets*, *Astron. Astrophys.*, *453*, 1129–1140.

Packham C., Honda M., Chun M. et al. (2018) in *Ground-based and Airborne Instrumentation for Astronomy VII* (C. J. Evans, L. Simard, and H. Takami, eds.), vol. 10702 of *Society of Photo-Optical Instrumentation Engineers (SPIE) Conference Series*, p. 10702A0.

Paneque-Carreño T., Izquierdo A. F., Teague R. et al. (2024) *High turbulence in the IM Lup protoplanetary disk. Direct observational constraints from CN and C_2H emission*, *Astron. Astrophys.*, *684*, A174.

Pegues J., Öberg K. I., Bergner J. B. et al. (2020) *An ALMA Survey of H_2CO in Protoplanetary Disks*, *Astrophys. J.*, *890*, 142.

Pérez L. M., Carpenter J. M., Chandler C. J. et al. (2012) *Constraints on the Radial Variation of Grain Growth in the AS 209 Circumstellar Disk*, *Astrophys. J. Lett.*, *760*, L17.

Pérez L. M., Chandler C. J., Isella A. et al. (2015) *Grain Growth in the Circumstellar Disks of the Young Stars CY Tau and DoAr 25*, *Astrophys. J.*, *813*, 41.

Phuong N. T., Chapillon E., Majumdar L. et al. (2018) *First detection of H_2S in a protoplanetary disk. The dense GG Tauri A ring*, *Astron. Astrophys.*, *616*, L5.

Phuong N. T., Dutrey A., Chapillon E. et al. (2021) *An unbiased NOEMA 2.6 to 4 mm survey of the GG Tau ring: First detection of CCS in a protoplanetary disk*, *Astron. Astrophys.*, *653*, L5.

Piani L., Tachibana S., Hama T. et al. (2017) *Evolution of Morphological and Physical Properties of Laboratory Interstellar Organic Residues with Ultraviolet Irradiation*, *Astrophys. J.*, *837*, 35.

Pineda J. E., Segura-Cox D., Caselli P. et al. (2020) *A protostellar system fed by a streamer of 10,500 au length*, *Nature Astronomy*, *4*, 1158–1163.

Pinilla P., Birnstiel T., Ricci L. et al. (2012) *Trapping dust particles in the outer regions of protoplanetary disks*, *Astron. Astrophys.*, *538*, A114.

Pinilla P., Pohl A., Stammler S. M. et al. (2017) *Dust Density Distribution and Imaging Analysis of Different Ice Lines in Protoplanetary Disks*, *Astrophys. J.*, *845*, 68.

Pinte C., Dent W. R. F., Ménard F. et al. (2016) *Dust and Gas in the Disk of HL Tauri: Surface Density, Dust Settling, and Dust-to-gas Ratio*, *Astrophys. J.*, *816*, 25.

Podio L., Garufi A., Codella C. et al. (2020) *ALMA chemical survey of disk-outflow sources in Taurus (ALMA-DOT). II. Vertical stratification of CO, CS, CN, H_2CO, and CH_3OH in a Class I disk*, *Astron. Astrophys.*, *642*, L7.

Pontoppidan K., Banzatti A., Bergin E. et al. (2019a) *The trail of water and the delivery of volatiles to habitable planets*, *Bull. Am. Astron. Soc.*, *51*, 229.

Pontoppidan K. M., Blake G. A., van Dishoeck E. F. et al. (2008) *Spectroastrometric Imaging of Molecular Gas within Protoplanetary Disk Gaps*, *Astrophys. J.*, *684*, 1323–1329.

Pontoppidan K. M. and Blevins S. M. (2014) *The chemistry of planet-forming regions is not interstellar*, *Faraday Discussions*, *168*, 49–60.

Pontoppidan K. M., Dullemond C. P., van Dishoeck E. F. et al. (2005) *Ices in the Edge-on Disk CRBR 2422.8-3423: Spitzer Spectroscopy and Monte Carlo Radiative Transfer Modeling*, *Astrophys. J.*, *622*, 463–481.

Pontoppidan K. M., Salyk C., Banzatti A. et al. (2019b) *The Nitrogen Carrier in Inner Protoplanetary Disks*, *Astrophys. J.*, *874*, 92.

Pontoppidan K. M., Salyk C., Banzatti A. et al. (2024) *High-contrast JWST-MIRI Spectroscopy of Planet-forming Disks for the JDISC Survey*, *Astrophys. J.*, *963*, 158.

Pontoppidan K. M., Salyk C., Blake G. A. et al. (2010) *A Spitzer Survey of Mid-infrared Molecular Emission from Protoplanetary Disks. I. Detection Rates*, *Astrophys. J.*, *720*, 887–903.

Qi C., D'Alessio P., Öberg K. I. et al. (2011) *Resolving the CO Snow Line in the Disk around HD 163296*, *Astrophys. J.*, *740*, 84.

Qi C., Kessler J. E., Koerner D. W. et al. (2003) *Continuum and CO/HCO^+ Emission from the Disk Around the T Tauri Star LkCa 15*, *Astrophys. J.*, *597*, 986–997.

Qi C., Öberg K. I., Espaillat C. C. et al. (2019) *Probing CO and N_2 Snow Surfaces in Protoplanetary Disks with N_2H^+ Emission*, *Astrophys. J.*, *882*, 160.

Qi C., Öberg K. I., Wilner D. J. et al. (2013a) *Imaging of the CO Snow Line in a Solar Nebula Analog*, *Science*, *341*, 630–632.

Qi C., Öberg K. I., Wilner D. J. et al. (2013b) *First Detection of c-C_3H_2 in a Circumstellar Disk*, *Astrophys. J. Lett.*, *765*, L14.

Qi C., Wilner D. J., Aikawa Y. et al. (2008) *Resolving the Chemistry in the Disk of TW Hydrae. I. Deuterated Species*, *Astrophys. J.*, *681*, 1396–1407.

Raettig N., Lyra W., and Klahr H. (2021) *Pebble Trapping in Vortices: Three-dimensional Simulations*, *Astrophys. J.*, *913*, 92.

Ricci L., Testi L., Natta A. et al. (2010a) *Dust grain growth in ρ-Ophiuchi protoplanetary disks*, *Astron. Astrophys.*, *521*, A66.

Ricci L., Testi L., Natta A. et al. (2010b) *Dust properties of protoplanetary disks in the Taurus-Auriga star forming region from millimeter wavelengths*, *Astron. Astrophys.*, *512*, A15.

Ritchey A. M., Federman S. R., and Lambert D. L. (2015) *The $C^{14}N/C^{15}N$ Ratio in Diffuse Molecular Clouds*, *Astrophys. J. Lett.*, *804*, L3.

Rivière-Marichalar P., Fuente A., Le Gal R. et al. (2021) *H_2S observations in young stellar disks in Taurus*, *Astron. Astrophys.*, *652*, A46.

Rosenfeld K. A., Andrews S. M., Hughes A. M. et al. (2013) *A Spatially Resolved Vertical Temperature Gradient in the HD 163296 Disk*, *Astrophys. J.*, *774*, 16.

Rosotti G. P., Teague R., Dullemond C. et al. (2020) *The efficiency of dust trapping in ringed protoplanetary discs*, *Mon. Not. R. Astron. Soc.*, *495*, 173–181.

Roueff E., Loison J. C., and Hickson K. M. (2015) *Isotopic fractionation of carbon, deuterium, and nitrogen: a full chemical study*, *Astron. Astrophys.*, *576*, A99.

Ruíz-Rodríguez D., Kastner J., Hily-Blant P. et al. (2021) *Tracing molecular stratification within an edge-on protoplanetary disk*, *Astron. Astrophys.*, *646*, A59.

Rybicki G. B. and Lightman A. P. (1979) *Radiative processes in astrophysics*, Wiley, New York.

Sadavoy S. I., Myers P. C., Stephens I. W. et al. (2018) *Dust Polarization toward Embedded Protostars in Ophiuchus with ALMA. I. VLA 1623*, *Astrophys. J.*, *859*, 165.

Sai J., Ohashi N., Saigo K. et al. (2020) *Disk Structure around the Class I Protostar L1489 IRS Revealed by ALMA: A Warped-disk System*, *Astrophys. J.*, *893*, 51.

Saito E. and Sirono S.-i. (2011) *Planetesimal Formation by Sublimation*, *Astrophys. J.*, *728*, 20.

Sakai N., Hanawa T., Zhang Y. et al. (2019) *A warped disk around an infant protostar*, *Nature*, *565*, 206–208.

Sakai N., Oya Y., Sakai T. et al. (2014) *A Chemical View of Protostellar-disk Formation in L1527*, *Astrophys. J. Lett.*, *791*, L38.

Salinas V. N., Hogerheijde M. R., Bergin E. A. et al. (2016) *First detection of gas-phase ammonia in a planet-forming disk. NH_3, N_2H^+, and H_2O in the disk around TW Hydrae*, *Astron. Astrophys.*, *591*, A122.

Salinas V. N., Hogerheijde M. R., Mathews G. S. et al. (2017) *DCO^+, DCN, and N_2D^+ reveal three different deuteration regimes in the disk around the Herbig Ae star HD 163296*, *Astron. Astrophys.*, *606*, A125.

Salyk C., Pontoppidan K. M., Blake G. A. et al. (2008) *H_2O and OH Gas in the Terrestrial Planet-forming Zones of Protoplanetary Disks*, *Astrophys. J. Lett.*, *676*, L49.

Salyk C., Pontoppidan K. M., Blake G. A. et al. (2011) *A Spitzer Survey of Mid-infrared Molecular Emission from Protoplanetary Disks. II. Correlations and Local Thermal Equilibrium Models*, *Astrophys. J.*, *731*, 130.

Sano T., Miyama S. M., Umebayashi T. et al. (2000) *Magnetorotational Instability in Protoplanetary Disks. II. Ionization State and Unstable Regions*, *Astrophys. J.*, *543*, 486–501.

Sasselov D. D. and Lecar M. (2000) *On the Snow Line in Dusty Protoplanetary Disks*, *Astrophys. J.*, *528*, 995–998.

Schoonenberg D., Okuzumi S., and Ormel C. W. (2017) *What pebbles are made of: Interpretation of the V883 Ori disk*, *Astron. Astrophys.*, *605*, L2.

Schoonenberg D. and Ormel C. W. (2017) *Planetesimal formation near the snowline: in or out?*, *Astron. Astrophys.*, *602*, A21.

Semenov D. and Wiebe D. (2011) *Chemical Evolution of Turbulent Protoplanetary Disks and the Solar Nebula*, *Astrophys. J. Suppl.*, *196*, 25.

Shibata K. and Uchida Y. (1986) *A magnetohydrodynamic mechanism for the formation of astrophysical jets. II. Dynamical processes in the accretion of magnetized mass in rotation.*, *PASJ*, *38*, 631–660.

Shingledecker C. N., Tennis J., Le Gal R. et al. (2018) *On Cosmic-Ray-driven Grain Chemistry in Cold Core Models*, *Astrophys. J.*, *861*, 20.

Shinnaka Y., Kawakita H., and Tajitsu A. (2020) *High-resolution Optical Spectroscopic Observations of Comet 21P/Giacobini-Zinner in Its 2018 Apparition*, *AJ*, *159*, 203.

Sierra A. and Lizano S. (2020) *Effects of Scattering, Temperature Gradients, and Settling on the Derived Dust Properties of Observed Protoplanetary Disks*, *Astrophys. J.*, *892*, 136.

Sierra A., Pérez L. M., Zhang K. et al. (2021) *Molecules with ALMA at Planet-forming Scales (MAPS). XIV. Revealing Disk Substructures in Multiwavelength Continuum Emission*, *Astrophys. J. Suppl.*, *257*, 14.

Simon J. B., Bai X.-N., Armitage P. J. et al. (2013a) *Turbulence in the Outer Regions of Protoplanetary Disks. II. Strong Accretion Driven by a Vertical Magnetic Field*, *Astrophys. J.*, *775*, 73.

Simon J. B., Bai X.-N., Stone J. M. et al. (2013b) *Turbulence in the Outer Regions of Protoplanetary Disks. I. Weak Accretion with No Vertical Magnetic Flux*, *Astrophys. J.*, *764*, 66.

Sirono S.-i. (2011) *Planetesimal Formation Induced by Sintering*, *Astrophys. J. Lett.*, *733*, L41.

Smith R. L., Pontoppidan K. M., Young E. D. et al. (2009) *High-Precision $C^{17}O$, $C^{18}O$, and $C^{16}O$ Measurements in Young Stellar Objects: Analogues for Co Self-shielding in the Early Solar System*, *Astrophys. J.*, *701*, 163–175.

Soon K.-L., Momose M., Muto T. et al. (2019) *Investigating the gas-to-dust ratio in the protoplanetary disk of HD 142527*, *PASJ*, *71*, 124.

Steinpilz T., Teiser J., and Wurm G. (2019) *Sticking Properties of Silicates in Planetesimal Formation Revisited*, *Astrophys. J.*, *874*, 60.

Stephens I. W., Looney L. W., Kwon W. et al. (2014) *Spatially resolved magnetic field structure in the disk of a T Tauri star*, *Nature*, *514*, 597–599.

Stephens I. W., Yang H., Li Z.-Y. et al. (2017) *ALMA Reveals Transition of Polarization Pattern with Wavelength in HL Tau's Disk*, *Astrophys. J.*, *851*, 55.

Suriano S. S., Li Z.-Y., Krasnopolsky R. et al. (2018) *The formation of rings and gaps in magnetically coupled disc-wind systems: ambipolar diffusion and reconnection*, *Mon. Not. R. Astron. Soc.*, *477*, 1239–1257.

Tabone B., Bettoni G., van Dishoeck E. F. et al. (2023) *A rich hydrocarbon chemistry and high C to O ratio in the inner disk around a very low-mass star*, *Nature Astronomy*, *7*, 805–814.

Takeuchi T., Clarke C. J., and Lin D. N. C. (2005) *The Differential Lifetimes of Protostellar Gas and Dust Disks*, *Astrophys. J.*, *627*, 286–292.

Takeuchi T. and Okuzumi S. (2014) *Radial Transport of Large-scale Magnetic Fields in Accretion Disks. II. Relaxation to Steady States*, *Astrophys. J.*, *797*, 132.

Tanaka H., Himeno Y., and Ida S. (2005) *Dust Growth and Settling in Protoplanetary Disks and Disk Spectral Energy Distributions. I. Laminar Disks*, *Astrophys. J.*, *625*, 414–426.

Tazaki R., Tanaka H., Kataoka A. et al. (2019) *Unveiling Dust Aggregate Structure in Protoplanetary Disks by Millimeter-wave Scattering Polarization*, *Astrophys. J.*, *885*, 52.

Tazzari M., Testi L., Ercolano B. et al. (2016) *Multiwavelength analysis for interferometric (sub-)mm observations of protoplanetary disks. Radial constraints on the dust properties and the disk structure*, *Astron. Astrophys.*, *588*, A53.

Teague R., Bae J., and Bergin E. A. (2019) *Meridional flows in the disk around a young star*, *Nature*, *574*, 378–381.

Teague R., Guilloteau S., Semenov D. et al. (2016) *Measuring turbulence in TW Hydrae with ALMA: methods and limitations*, *Astron. Astrophys.*, *592*, A49.

Teague R., Henning T., Guilloteau S. et al. (2018) *Temperature, Mass, and Turbulence: A Spatially Resolved Multiband Non-LTE Analysis of CS in TW Hya*, *Astrophys. J.*, *864*, 133.

Teague R. and Loomis R. (2020) *The Excitation Conditions of CN in TW Hya*, *Astrophys. J.*, *899*, 157.

Teague R., Semenov D., Guilloteau S. et al. (2015) *Chemistry in disks. IX. Observations and modelling of HCO^+ and DCO^+ in DM Tauri*, *Astron. Astrophys.*, *574*, A137.

Terada H., Tokunaga A. T., Kobayashi N. et al. (2007) *Detection of Water Ice in Edge-on Protoplanetary Disks: HK Tauri B and HV Tauri C*, *Astrophys. J.*, *667*, 303–307.

Testi L., Birnstiel T., Ricci L. et al. (2014) in *Protostars and Planets VI* (H. Beuther, R. S. Klessen, C. P. Dullemond, and T. Henning, eds.), p. 339.

Thi W. F., Ménard F., Meeus G. et al. (2011) *Detection of CH^+ emission from the disc around HD 100546*, *Astron. Astrophys.*, *530*, L2.

Tobin J. J., van't Hoff M. L. R., Leemker M. et al. (2023) *Deuterium-enriched water ties planet-forming disks to comets and protostars*, *Nature*, *615*, 227–230.

Tsukamoto Y., Maury A., Commercon B. et al. (2023) in *Astronomical Society of the Pacific Conference Series* (S. Inutsuka, Y. Aikawa, T. Muto, K. Tomida, and M. Tamura, eds.), vol. 534 of *Astronomical Society of the Pacific Conference Series*, p. 317.

Tsukamoto Y., Takahashi S. Z., Machida M. N. et al. (2015) *Effects of radiative transfer on the structure of self-gravitating discs, their fragmentation and the evolution of the fragments*, *Mon. Not. R. Astron. Soc.*, *446*, 1175–1190.

Turner N. J. and Sano T. (2008) *Dead Zone Accretion Flows in Protostellar Disks*, *Astrophys. J. Lett.*, *679*, L131.

Tychoniec Ł., van Dishoeck E. F., van't Hoff M. L. R. et al. (2021) *Which molecule traces what: Chemical diagnostics of protostellar sources*, *Astron. Astrophys.*, *655*, A65.

Ueda T., Kataoka A., Zhang S. et al. (2021) *Impact of Differential Dust Settling on the SED and Polarization: Application to the Inner Region of the HL Tau Disk*, *Astrophys. J.*, *913*, 117.

Urpin V. and Brandenburg A. (1998) *Magnetic and vertical shear instabilities in accretion discs*, *Mon. Not. R. Astron. Soc.*, *294*, 399–406.

van der Marel N., Booth A. S., Leemker M. et al. (2021) *A major asymmetric ice trap in a planet-forming disk. I. Formaldehyde and methanol*, *Astron. Astrophys.*, *651*, L5.

van der Marel N., Dong R., di Francesco J. et al. (2019) *Protoplanetary Disk Rings and Gaps across Ages and Luminosities*, *Astrophys. J.*, *872*, 112.

van Dishoeck E. F., Grant S., Tabone B. et al. (2023) *The diverse chemistry of protoplanetary disks as revealed by JWST*, *Faraday Discussions*, *245*, 52–79.

van Dishoeck E. F., Herbst E., and Neufeld D. A. (2013) *Interstellar Water Chemistry: From Laboratory to Observations*, *Chemical Reviews*, *113*, 9043–9085.

van Dishoeck E. F., Kristensen L. E., Mottram J. C. et al. (2021) *Water in star-forming regions: physics and chemistry from clouds to disks as probed by Herschel spectroscopy*, *Astron. Astrophys.*, *648*, A24.

van Dishoeck E. F., Thi W. F., and van Zadelhoff G. J. (2003) *Detection of DCO^+ in a circumstellar disk*, *Astron. Astrophys.*, *400*, L1–L4.

van't Hoff M. L. R., Harsono D., Tobin J. J. et al. (2020) *Temperature Structures of Embedded Disks: Young Disks in Taurus Are Warm*, *Astrophys. J.*, *901*, 166.

Visser R., Bruderer S., Cazzoletti P. et al. (2018) *Nitrogen isotope fractionation in protoplanetary disks*, *Astron. Astrophys.*, *615*, A75.

Visser R., Doty S. D., and van Dishoeck E. F. (2011) *The chemical history of molecules in circumstellar disks. II. Gas-phase species*, *Astron. Astrophys.*, *534*, A132.

Visser R., van Dishoeck E. F., Doty S. D. et al. (2009) *The chemical history of molecules in circumstellar disks. I. Ices*, *Astron. Astrophys.*, *495*, 881–897.

Wada K., Tanaka H., Suyama T. et al. (2009) *Collisional Growth Conditions for Dust Aggregates*, *Astrophys. J.*, *702*, 1490–1501.

Walsh C., Loomis R. A., Öberg K. I. et al. (2016) *First Detection of Gas-phase Methanol in a Protoplanetary Disk*, *Astrophys. J. Lett.*, *823*, L10.

Walsh C., Nomura H., and van Dishoeck E. (2015) *The molecular composition of the planet-forming regions of protoplanetary disks across the luminosity regime*, *Astron. Astrophys.*, *582*, A88.

Wang H., Weiss B. P., Bai X.-N. et al. (2017) *Lifetime of the solar nebula constrained by meteorite paleomagnetism*, *Science*, *355*, 623–627.

Wardle M. (2007) *Magnetic fields in protoplanetary disks*, *Astrophys. Space Sci.*, *311*, 35–45.

Warren S. G. (1984) *Optical constants of ice from the ultraviolet to the microwave*, *Appl. Opt.*, *23*, 1206–1225.

Weidenschilling S. J. (1977) *Aerodynamics of solid bodies in the solar nebula.*, *Mon. Not. R. Astron. Soc.*, *180*, 57–70.

Weidenschilling S. J. (1980) *Dust to planetesimals: Settling and coagulation in the solar nebula*, *Icarus*, *44*, 172–189.

Weintraub D. A., Kastner J. H., and Bary J. S. (2000) *Detection of Quiescent Molecular Hydrogen Gas in the Circumstellar Disk of a Classical T Tauri Star*, *Astrophys. J.*, *541*, 767–771.

Weintraub D. A., Sandell G., and Duncan W. D. (1989) *Submillimeter Measurements of T Tauri and FU Orionis Stars*, *Astrophys. J. Lett.*, *340*, L69.

Whipple F. L. (1972) in *From Plasma to Planet* (A. Elvius, ed.), p. 211.

White R. J., Greene T. P., Doppmann G. W. et al. (2007) in *Protostars and Planets V* (B. Reipurth, D. Jewitt, and K. Keil, eds.), p. 117.

Whittet D. C. B. (1993) in *Dust and Chemistry in Astronomy* (T. J. Millar and D. A. Williams, eds.), p. 9.

Willacy K. (2007) *The Chemistry of Multiply Deuterated Molecules in Protoplanetary Disks. I. The Outer Disk*, *Astrophys. J.*, *660*, 441–460.

Yamamoto T., Nakagawa N., and Fukui Y. (1983) *The chemical composition and thermal history of the ice of a cometary nucleus*, *Astron. Astrophys.*, *122*, 171–176.

Yamato Y., Aikawa Y., Guzmán V. V. et al. (2024a) *Detection of Dimethyl Ether in the Central Region of the MWC 480 Protoplanetary Disk*, *Astrophys. J.*, *974*, 83.

Yamato Y., Notsu S., Aikawa Y. et al. (2024b) *Chemistry of Complex Organic Molecules in the V883 Ori Disk Revealed by ALMA Band 3 Observations*, *Astron. J.*, *167*, 66.

Yang H. and Li Z.-Y. (2020) *The Effects of Dust Optical Properties on the Scattering-induced Disk Polarization by Millimeter-sized Grains*, *Astrophys. J.*, *889*, 15.

Yang H., Li Z.-Y., Looney L. et al. (2016) *Inclination-induced polarization of scattered millimetre radiation from protoplanetary discs: the case of HL Tau*, *Mon. Not. R. Astron. Soc.*, *456*, 2794–2805.

Yang L., Ciesla F. J., and Alexander C. M. O. D. (2013) *The D/H ratio of water in the solar nebula during its formation and evolution*, *Icarus*, *226*, 256–267.

Yen H.-W., Takakuwa S., Ohashi N. et al. (2014) *ALMA Observations of Infalling Flows toward the Keplerian Disk around the Class I Protostar L1489 IRS*, *Astrophys. J.*, *793*, 1.

Yoneda H., Tsukamoto Y., Furuya K. et al. (2016) *Chemistry in a Forming Protoplanetary Disk: Main Accretion Phase*, *Astrophys. J.*, *833*, 105.

Yoshida T. C., Nomura H., Furuya K. et al. (2022) *A New Method for Direct Measurement of Isotopologue Ratios in Protoplanetary Disks: A Case Study of the* ^{12}*CO/*^{13}*CO Ratio in the TW Hya Disk*, *Astrophys. J.*, *932*, 126.

Yurimoto H. and Kuramoto K. (2004) *Molecular Cloud Origin for the Oxygen Isotope Heterogeneity in the Solar System*, *Science*, *305*, 1763–1766.

Zhang K., Bergin E. A., Blake G. A. et al. (2017) *Mass inventory of the giant-planet formation zone in a solar nebula analogue*, *Nature Astronomy*, *1*, 0130.

Zhang K., Bergin E. A., Schwarz K. et al. (2019) *Systematic Variations of CO Gas Abundance with Radius in Gas-rich Protoplanetary Disks*, *Astrophys. J.*, *883*, 98.

Zhang K., Blake G. A., and Bergin E. A. (2015) *Evidence of Fast Pebble Growth Near Condensation Fronts in the HL Tau Protoplanetary Disk*, *Astrophys. J. Lett.*, *806*, L7.

Zhang K., Booth A. S., Law C. J. et al. (2021) *Molecules with ALMA at Planet-forming Scales (MAPS). V. CO Gas Distributions*, *Astrophys. J. Suppl.*, *257*, 5.

Zhang K., Pontoppidan K. M., Salyk C. et al. (2013) *Evidence for a Snow Line beyond the Transitional Radius in the TW Hya Protoplanetary Disk*, *Astrophys. J.*, *766*, 82.

Zhang K., Schwarz K. R., and Bergin E. A. (2020) *Rapid Evolution of Volatile CO from the Protostellar Disk Stage to the Protoplanetary Disk Stage*, *Astrophys. J. Lett.*, *891*, L17.

Zhu Z. and Stone J. M. (2018) *Global Evolution of an Accretion Disk with a Net Vertical Field: Coronal Accretion, Flux Transport, and Disk Winds*, *Astrophys. J.*, *857*, 34.

Zhu Z., Zhang S., Jiang Y.-F. et al. (2019) *One Solution to the Mass Budget Problem for Planet Formation: Optically Thick Disks with Dust Scattering*, *Astrophys. J. Lett.*, *877*, L18.

Zsom A., Ormel C. W., Güttler C. et al. (2010) *The outcome of protoplanetary dust growth: pebbles, boulders, or planetesimals? II. Introducing the bouncing barrier*, *Astron. Astrophys.*, *513*, A57.

This 2-column preprint was prepared with the AAS LaTeX macros v5.2.

Table 1: Molecules detected in Class II disks[a]

species	wavelength	references (e.g.)	species	wavelength	references (e.g.)
H_2	NIR and MIR	[1][2]	HD	FIR	[3][4]
CH^+	FIR	[5][6]	OH	NIR, MIR, FIR	[6][7]
CN	sub-mm, mm	[8] [9]	^{13}CN	mm	[53]
$C^{15}N$	sub-mm	[10]	CO	NIR, MIR, FIR, sub-mm, mm	[8] [11]
^{13}CO	NIR, FIR, sub-mm, mm	[8] [12]	$C^{17}O$	NIR, sub-mm	[9] [13]
$C^{18}O$	NIR, sub-mm, mm	[12] [14]	$^{13}C^{18}O$	sub-mm	[14]
$^{13}C^{17}O$	sub-mm	[15]	NO	submm	[54]
CS	mm	[8] [17]	^{13}CS	mm	[17] [18]
$C^{34}S$	mm	[8] [17]	SO	sub-mm, mm	[19] [20]
H_2O	NIR, MIR, FIR, sub-mm	[7] [21] [22]	HDO	mm	[55]
$H_2^{18}O$	mm	[55]	C_2H	mm	[8] [24]
C_2D	mm	[18]	HCN	NIR, MIR, sub-mm, mm	[23] [24]
$H^{13}CN$	sub-mm, mm	[25] [23]	$HC^{15}N$	sub-mm	[23]
DCN	mm	[26] [27]	HNC	mm	[8] [28]
DNC	sub-mm	[18]	HCO^+	sub-mm, mm	[8] [29]
DCO^+	sub-mm, mm	[30] [27]	$H^{13}CO^+$	sub-mm, mm	[30] [25]
$HC^{18}O^+$	sub-mm	[31]	N_2H^+	mm	[32] [33]
N_2D^+	mm	[34] [35]	H_2S	mm	[36] [37]
CO_2	MIR	[16][56]	$^{13}CO_2$	MIR	[56]
C_2S	mm	[53]	OCS	mm	[60]
SO_2	sub-mm	[38]	$^{34}SO_2$	sub-mm	[38]
NH_3	MIR, sub-mm	[39][58]	C_2H_2	NIR, MIR	[40] [56]
$^{13}C^{12}CH_2$	MIR	[57]	H_2CO	sub-mm, mm	[8] [41]
H_2CS	sub-mm, mm	[17] [18]	HC_3N	mm	[42] [43]
HCOOH	mm	[44]	$c-C_3H_2$	mm	[45] [43]
CH_4	NIR	[46]	CH_2CN	mm	[47]
CH_3CN	mm	[48] [43]	CH_3OH	sub-mm, mm	[49] [50]
C_4H_2	MIR	[57]	CH_3CHO	submm	[52]
CH_3OCHO	submm	[51] [52]	$^{13}CH_3OCHO$	mm	[60]
$CH_3O^{13}CHO$	mm	[60]	CH_3OCH_3	submm	[51] [59]
CH_3COCH_3	submm	[52]	$t-C_2H_3CHO$	mm	[60]
$s-C_2H_5CHO$	mm	[60]	C_6H_6	MIR	[57]

[a] Adopted and revised from *McGuire* (2018). This table includes molecules detected in the disk of V883 Ori, which is a Class I object in outburst phase (section 4.2). The range of wavelengths are 2-5 μm for near-indrared (NIR), 5-40 μm for mid-infrared (MIR), 40-300 μm for far-infrared (FIR), 300-1000 μm for sub-millimeter (sub-mm), and $\geq$ 1 mm for millimeter (mm). References are not exhaustive. In addition to the first detection papers, we list recent papers for readers to refer to references therein (see also text).

References: [1] *Weintraub et al.* (2000) [2] *Martin-Zaïdi et al.* (2007) [3] *Bergin et al.* (2013) [4]*McClure et al.* (2016) [5] *Thi et al.* (2011) [6] *Fedele et al.* (2013) [7] *Salyk et al.* (2008) [8] *Dutrey et al.* (1997) [9] *Guilloteau et al.* (2013) [10] *Hily-Blant et al.* (2017) [11] *Najita et al.* (2003) [12] *Ansdell et al.* (2016) [13] *Qi et al.* (2011) [14] *Zhang et al.* (2017) [15] *Booth et al.* (2019) [16] *Carr and Najita* (2008) [17] *Le Gal et al.* (2019) [18] *Loomis et al.* (2020) [19] *Fuente et al.* (2010) [20] *Booth et al.* (2018) [21] *Carr et al.* (2004) [22] *Hogerheijde et al.* (2011) [23] *Hily-Blant et al.* (2019) [24] *Guzmán et al.* (2021) [25] *Huang et al.* (2017) [26] *Qi et al.* (2008) [27] *Öberg et al.* (2021a) [28] *Long et al.* (2021) [29] *Aikawa et al.* (2021) [30] *van Dishoeck et al.* (2003) [31] *Furuya et al.* (2022b) [32] *Qi et al.* (2003) [33] *Qi et al.* (2019) [34] *Huang and Öberg* (2015) [35] *Cataldi et al.* (2021) [36] *Phuong et al.* (2018) [37] *Rivière-Marichalar et al.* (2021) [38] *Booth et al.* (2021a) [39] *Salinas et al.* (2016) [40] *Lahuis et al.* (2006) [41] *Pegues et al.* (2020) [42] *Chapillon et al.* (2012) [43] *Ilee et al.* (2021) [44] *Favre et al.* (2018) [45] *Qi et al.* (2013b) [46] *Gibb and Horne* (2013) [47] *Canta et al.* (2021) [48] *Öberg et al.* (2015) [49] *Walsh et al.* (2016) [50] *van der Marel et al.* (2021) [51] *Brunken et al.* (2022) [52] *Lee et al.* (2019) [53] *Phuong et al.* (2021) [54] *Leemker et al.* (2023) [55] *Tobin et al.* (2023) [56] *Grant et al.* (2023) [57] *Tabone et al.* (2023) [58] *Najita et al.* (2021) [59] *Yamato et al.* (2024a) [60] *Yamato et al.* (2024b)

Table 2: Molecular D/H ratios measured in Class II disks and comets

object	DCO^+/HCO^+	N_2D^+/N_2H^+	DCN/HCN
DM Tau	0.1 (50 au) − 0.2 (450 au)[a]		
TW Hya	0.01 (30 au) − 0.1 (70 au)[b]		0.17[c]
AS 209	0.037-0.08[d]	0.3-0.5[e]	0.028-0.059[d]
		0.67-0.94 (159 au)[f]	0.074-0.092 (118 au)[f]
IM Lup	0.023-0.037[d]		0.043-0.074[d]
		0.28-0.37 (76 au)[f]	0.17-0.24 (367 au)[f]
V4046 Sgr	0.014-0.029[d]		0.004-0.008[d]
LkCa15	0.019-0.038[d]		0.04-0.12[d]
GM Aur		< 0.064 (216 au)[f]	0.079-0.13 (298 au) [f]
MWC 480	0.021-0.043[d]		0.006-0.018[d]
		0.40-0.66 (143 au)[f]	0.055-0.094 (133 au)[f]
HD 163296	0.039-0.075[d]		0.012-0.027[d]
	0.04-0.07[g]	0.19-0.66[g]	0.01-0.03[g]
		1.29-1.72 (152 au)[f]	0.048-0.062 (129 au)[f]
comet Hale-Bopp			$(2.3 \pm 0.4) \times 10^{-3}$[h]

[a] *Teague et al.* (2015)
[b] *Qi et al.* (2008)
[c] disk average (*Öberg et al.* 2012)
[d] disk average (*Huang et al.* 2017)
[e] disk average (*Huang and Öberg* 2015)
[f] peak value in the radial distribution (*Cataldi et al.* 2021)
[g] disk average (*Salinas et al.* 2017)
[h] *Meier et al.* (1998); *Crovisier et al.* (2004)

Table 3: Molecular $^{14}N/^{15}N$ ratios measured in Class II disks and comets

object	$HC^{14}N/HC^{15}N$	$C^{14}N/C^{15}N$
TW Hya	223 ± 21[a]	323 ± 30[a]
	121 ± 11 (20 au) -339 ± 21 (45 au)[b]	
AS 209	156 ± 71[c]	
V4046 Sgr	115 ± 35[c]	
LkCa15	83 ± 32[c]	
MWC 480	123 ± 45[c]	
HD 163296	142 ± 59[c]	
comet Hale-Bopp	205 ± 70[d]	140 ± 35[e]
comet 17P/Holmes	139 ± 26[d]	165 ± 40[d]

[a] disk average (*Hily-Blant et al.* 2019)
[b] radial distribution (*Hily-Blant et al.* 2019)
[c] disk average (*Guzmán et al.* 2017)
[d] *Bockelée-Morvan et al.* (2008)
[e] *Arpigny et al.* (2003)